JOURNAL OF PETROLOGY | VOLUME 47 | NUMBER 4 | PAGES 647–671 | 2006 | doi:10.1093/petrology/egi088

Immiscible Transition from Carbonate-rich to Silicate-rich Melts in the 3 GPa Melting Interval of Eclogite + CO_2 and Genesis of Silica-undersaturated Ocean Island Lavas

RAJDEEP DASGUPTA*, MARC M. HIRSCHMANN AND KATHRYN STALKER

DEPARTMENT OF GEOLOGY AND GEOPHYSICS, UNIVERSITY OF MINNESOTA, 310 PILLSBURY DRIVE SE, MINNEAPOLIS, MN 55455, USA

RECEIVED APRIL 25, 2005; ACCEPTED OCTOBER 27, 2005; ADVANCE ACCESS PUBLICATION DECEMBER 7, 2005

We explore the partial melting behavior of a carbonated silica-deficient eclogite (SLEC1; 5 wt % CO_2) from experiments at 3 GPa and compare the compositions of partial melts with those of alkalic and highly alkalic oceanic island basalts (OIBs). The solidus is located at 1050–1075°C and the liquidus at ~1415°C. The sub-solidus assemblage consists of clinopyroxene, garnet, ilmenite, and calcio-dolomitic solid solution and the near solidus melt is carbonatitic (<2 wt % SiO_2, <1 wt % Al_2O_3, and <0·1 wt % TiO_2). Beginning at 1225°C, a strongly silica-undersaturated silicate melt (~34–43 wt % SiO_2) with high TiO_2 (up to 19 wt %) coexists with carbonate-rich melt (<5 wt % SiO_2). The first appearance of carbonated silicate melt is ~100°C cooler than the expected solidus of CO_2-free eclogite. In contrast to the continuous transition from carbonate to silicate melts observed experimentally in peridotite + CO_2 systems, carbonate and silicate melt coexist over a wide temperature interval for partial melting of SLEC1 carbonated eclogite at 3 GPa. Silicate melts generated from SLEC1, especially at high melt fraction (>20 wt %), may be plausible sources or contributing components to melilitites and melilititic nephelinites from oceanic provinces, as they have strong compositional similarities including their SiO_2, FeO, MgO, CaO, TiO_2 and Na_2O contents, and CaO/Al_2O_3 ratios. Carbonated silicate partial melts from eclogite may also contribute to less extreme alkalic OIB, as these lavas have a number of compositional attributes, such as high TiO_2 and FeO* and low Al_2O_3, that have not been observed from partial melting of peridotite ± CO_2. In upwelling mantle, formation of carbonatite and silicate melts from eclogite and peridotite source lithologies occurs over a wide range of depths, producing significant opportunities for metasomatic transfer and implantation of melts.*

KEY WORDS: *carbonated eclogite; experimental phase equilibria; partial melting; liquid immiscibility; ocean island basalts*

INTRODUCTION

Silica-undersaturated lavas are characteristic of many intraplate magmatic provinces, including those on continents (e.g. Wilson *et al.*, 1995; Janney *et al.*, 2002) and on many oceanic islands (e.g. Clague & Frey, 1982; Hoernle & Schmincke, 1993; Kogiso *et al.*, 1997). Such lavas have conventionally been believed to originate from small degrees of partial melting of fertile peridotite, possibly in the presence of small amounts of CO_2 ± H_2O (e.g. Eggler, 1978; Hémond *et al.*, 1994). However, detailed experimental studies documenting a link between such partial melts and alkalic lavas are incomplete, and many questions remain regarding their petrogenesis.

Alkalic lavas from oceanic islands have a wide range of compositions (Fig. 1) that presumably reflect a spectrum of sources and processes. As noted recently by Hirschmann *et al.* (2003) and Kogiso *et al.* (2003), key compositional characteristics of some alkalic oceanic island basalts (OIBs) differ significantly from liquids likely to be descended from those generated in existing experimental partial melting studies of peridotite (e.g. Hirose & Kushiro, 1993; Walter, 1998). This may be simply because such magmas are generated at very small degrees of melting of garnet peridotite, and experiments at the appropriately low melt fraction have yet to be achieved.

*Corresponding author. Telephone: +1-612-625-0366. Fax: +1-612-625-3819. E-mail: dasg0007@umn.edu

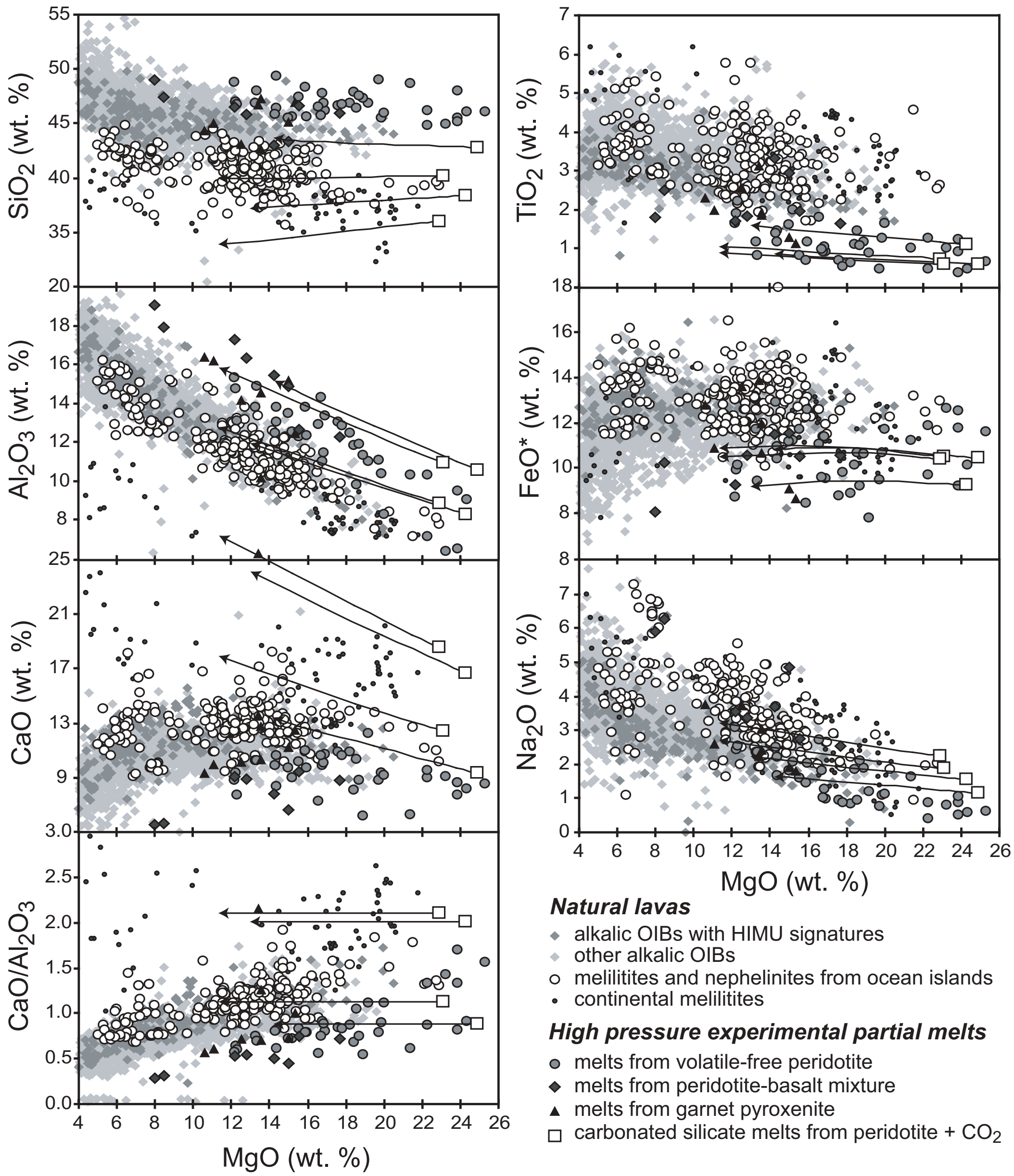

Fig. 1. Compositions of melilitites and nephelinites from oceanic islands, and melilitites from continental provinces compared with high-pressure experimental partial melts of various potential mantle assemblages. Also included for comparison are ocean island basalts (OIB) with HIMU signatures and other primitive alkalic OIBs from the compilation of Kogiso *et al.* (2003). Oceanic melilitite and nephelinite [after classification of Le Bas (1989)] lavas are from Austral-Cook (Dupuy *et al.*, 1988, 1989; Caroff *et al.*, 1997; GEOROC database: http://georoc.mpch-mainz.gwdg.de/georoc/), Canaries (Hoernle & Schmincke, 1993; Demény *et al.*, 2004), Cape Verde (Jørgensen & Holm, 2002; Doucelance *et al.*, 2003; GEOROC database), Comoros (Nougier *et al.*, 1986; Späth *et al.*, 1996), Fernando de Noronha (Weaver, 1990; GEOROC database), Hawaii (Clague & Frey, 1982; Clague & Dalrymple, 1988; Maaløe *et al.*, 1992; Dixon *et al.*, 1997), Samoa (Hawkins & Natland, 1975; Palacz & Saunders, 1986; Workman *et al.*, 2004) and Trindade (Oversby, 1971; Weaver, 1990; GEOROC database). Compositions of mafic (MgO >4 wt %) alkalic OIBs are from Azores, Tristan de Cunha, Society, Samoa, Pitcairn, Marquesas, Cook–Austral, and Canaries. Ocean island lavas with HIMU signatures are from Mangaia, Rurutu, and Tubuai from Cook–Austral and St. Helena. Selected data for continental melilitites are from Brey (1978), Frey *et al.* (1978), Dawson *et al.* (1985), Hegner *et al.* (1995), Wilson *et al.* (1995), Nielsen *et al.* (1997), Ivanikov *et al.* (1998), Janney *et al.* (2002), and Schultz *et al.* (2004). All natural lava compositions are normalized volatile-free. Experimental silicate-rich partial melts are from fertile peridotite between 2·5 and 7·0 GPa (Takahashi & Kushiro, 1983; Takahashi, 1986; Hirose & Kushiro, 1993; Kushiro, 1996; Walter, 1998), garnet pyroxenite between 2·0 and 5·0 GPa (Hirschmann *et al.*, 2003; Kogiso *et al.*, 2003), peridotite–basalt mixture between 1·5 and 2·0 GPa (Kogiso *et al.*, 1998), and peridotite + CO_2 at 3·0 GPa (Hirose, 1997). Arrows represent olivine fractionation trends of up to 35% from partial melts of Hirose (1997), using Fe^{2+}–Mg $K_D = 0{\cdot}33$–$0{\cdot}39$, determined from the same experiments (Hirose, 1997). This model of olivine extraction assumes fractionation of high-pressure liquids at shallow depths. Fractionation at intermediate pressures may involve cpx; however, such a process would not bring the trajectories closer to the target lava compositions.

On the other hand, associations between these lavas and isotopic signatures of crustal recycling (e.g. Hoernle *et al.*, 1991; Kogiso *et al.*, 1997; Janney *et al.*, 2002; Jørgensen & Holm, 2002; Doucelance *et al.*, 2003; Workman *et al.*, 2004) have induced exploration of the hypothesis that the major element compositions of these lavas reflect a component derived from partial melts of pyroxenite or eclogite (Hirschmann *et al.*, 2003; Kogiso *et al.*, 2003). Similarly, a role for CO_2 should be considered, as lavas from these provinces show evidence for high CO_2 (e.g. Dixon *et al.*, 1997), and their mantle source regions may be affected by CO_2-rich fluids and/or carbonatitic melts (Hauri *et al.*, 1993; Saal *et al.*, 1998; Coltorti *et al.*, 1999; Kogarko *et al.*, 2001; Neumann *et al.*, 2002). In some localities, alkalic OIBs are associated with crustally emplaced carbonatites (e.g. Allègre *et al.*, 1971; Hoernle *et al.*, 2002).

Highly silica-undersaturated lavas such as melilitite and melilititic nephelinite (Le Bas, 1989) occur on some oceanic islands (e.g. Clague & Frey, 1982; Maaløe *et al.*, 1992; Hoernle & Schmincke, 1993; Jørgensen & Holm, 2002; Doucelance *et al.*, 2003; Demény *et al.*, 2004). These lavas are characterized by much lower silica contents (Fig. 1) than those found in partial melting experiments of volatile-poor peridotite (Fig. 1). Many also carry distinctive trace element and radiogenic isotopic signatures similar to the HIMU mantle component (e.g. Hoernle *et al.*, 1991; Jørgensen & Holm, 2002; Doucelance *et al.*, 2003) and, thus, may incorporate recycled crustal material at their source. Melilitites and melilitic nephelinites from continents are similar, both in their major element compositions and their signatures of crustal recycling (e.g. Wilson *et al.*, 1995; Janney *et al.*, 2002). Also, there is a strong association in the field between melilitites, CO_2, and carbonatites (e.g. Schultz *et al.*, 2004). Although volumetrically subordinate to more typical alkali basalt–basanite–nephelinite suites, these silica-poor alkalic lavas are of particular interest because experimental studies have so far failed to demonstrate equilibrium of melilititic melts with a four-phase (olivine + orthopyroxene + clinopyroxene + garnet) natural peridotite assemblage (Brey & Green, 1975, 1977; Brey, 1978; Brey & Ryabchikov, 1994).

Experiments investigating the possible role of carbonated eclogite in the petrogenesis of alkalic and highly alkalic OIB have not been performed previously. Here we present the results of partial melting experiments for a natural eclogite that has been modified by addition of carbonates (SLEC1; 5 wt % CO_2) at 3 GPa. In previous studies, we examined production of carbonatitic liquids from this carbonated eclogite (Dasgupta *et al.*, 2004, 2005*a*). In the present study, we extend these experiments to higher temperature to document the transition from lower temperature carbonatite partial melts to carbonated silicate partial melts and to investigate possible relationships between these melts and the origin of alkalic (alkali basalt–basanite–nephelinite) and highly alkalic (melilitite–melilite nephelinite) intraplate lavas. First, we briefly review some relevant constraints on the petrogenesis of these lavas.

Origin of alkalic oceanic island basalt suites

It is well established that partial melting of peridotite ± CO_2 at high pressure and sufficiently low melt fraction gives rise to nepheline-normative liquids with compositional similarities to alkali basalt–basanite–nephelinite suites common on oceanic islands (e.g. Takahashi & Kushiro, 1983; Hirose & Kushiro, 1993; Hirose, 1997; Green & Falloon, 1998). However, in detail, liquids generated from existing experiments on peridotite ± CO_2 are distinct from many natural lavas in some important respects. For example, the lavas have lower Al_2O_3 and higher FeO* and TiO_2 at a given MgO concentration than liquids likely to be derived by crystal fractionation from partial melts of volatile-poor peridotite or from partial melts of carbonated peridotite (Fig. 1; see also Kogiso *et al.*, 2003). This may be because existing experiments on carbonated peridotite (Hirose, 1997) reflect relatively high degrees of melting. The compositions of small-degree partial melts of carbonated peridotite may possibly be more appropriate as parents for natural alkalic OIB suites.

As pointed out by Kogiso *et al.* (1998, 2003) and shown in Fig. 1, lavas with strong HIMU isotopic signatures of recycled oceanic crust are enriched in CaO and CaO/Al_2O_3 relative to experimental partial melts of volatile-poor peridotite. These must reflect contributions from CaO-rich melts, which may plausibly be related to the character of the HIMU source. Partial melts of carbonated peridotite are highly calcic, and, therefore, could play a role in HIMU genesis, although, as mentioned above, the lower FeO* and TiO_2 and higher Al_2O_3 concentrations of carbonated peridotite partial melts from the experiments of Hirose (1997) are not appropriate for parental melts of the HIMU or other alkalic OIB lavas.

Recently it has been shown that high-pressure partial melting of silica-deficient garnet pyroxenite (MIX1G) also generates silica-undersaturated lavas similar to alkalic OIBs (Hirschmann *et al.*, 2003; Kogiso *et al.*, 2003). However, MIX1G does not produce melts with silica and alumina as low as primitive alkalic OIB and, thus, Kogiso *et al.* (2003) suggested that a source composition more silica deficient than MIX1G or a carbonated garnet pyroxenite could be a better source lithology for OIB parental melts. Keshav *et al.* (2004) argued that garnet pyroxenite is not a plausible source lithology for alkalic OIB suites because partial melting trends are transverse to variations of alkalic OIBs on $MgO-Al_2O_3$ and $CaO-SiO_2$ diagrams. This would be a valid consideration if varying degrees of isobaric partial melting were the principal cause of compositional variation in such suites. But if the alkali OIB major element trends chiefly reflect some other process, such as fractionation and/or accumulation of mafic phenocrysts, then the obliquity of the partial melting and lava trends is not relevant.

Origin of melilitites and melilitite nephelinites

In addition to low SiO_2, melilitites and melilitic nephelinites are characterized by high TiO_2, FeO*, CaO, Na_2O and CaO/Al_2O_3 (Fig. 1). These cannot be derived by partial melting of peridotite in the absence of volatiles (e.g. Takahashi & Kushiro, 1983), but liquids with some of these compositional characteristics can be generated by partial melting of carbonated peridotite (Eggler, 1978; Hirose, 1997). For example, MgO-rich partial melts of carbonated peridotite produced at 3 GPa (Hirose, 1997) may evolve by olivine fractionation to liquids that match the SiO_2, CaO, Na_2O contents, and CaO/Al_2O_3, of melilitites and nephelinites (Fig. 1). However, these experimentally produced liquids are too poor in TiO_2 and FeO* and too rich in Al_2O_3 at a given MgO content to account for ocean island melilitite, melilite nephelinite, and continental melilitites (Fig. 1). Thus, compared with partial melts of peridotite or carbonated peridotite from known experiments, both common alkalic OIB and melilititic lavas seem to require sources capable of generating higher TiO_2 and FeO* and lower Al_2O_3. This may be why inverse experiments on the liquidus phase relations of olivine melilitite + H_2O + CO_2 for a range of upper mantle P, T, XH_2O, XCO_2, and fO_2 conditions failed to locate saturation with a lherzolite or harzburgite assemblage (Brey & Green, 1977; Brey, 1978). Instead, liquidus assemblages of primitive olivine melilitites at moderate to high pressures (0·5–3 GPa) include clinopyroxenite, garnet clinopyroxenite or wehrlite (Brey & Ryabchikov, 1994). Consequently, highly silica-undersaturated lavas may not be derived from sources consisting solely of typical carbonated natural lherzolite.

A key point is that much of the discussion regarding the origin of alkalic lavas has been based on comparisons between experimental partial melts and natural lavas projected into pseudo-ternary or pseudo-tetrahedral normative compositions (O'Hara, 1968). Although this is a powerful form of analysis, it has the potential to obscure key differences between experimental and natural liquids. For example, such projections do not address whether experimental partial melts have suitable FeO* for a given MgO concentration (Herzberg & O'Hara, 2002) or whether they are sufficiently rich in TiO_2 to be parental to natural melilititic–nephelinitic lavas. For this reason, comparisons in this paper will be made chiefly through major element variation diagrams.

Table 1: Composition of the starting material

	66039B	cpx	gt	SLEC1
SiO_2	46·34	50·27	40·66	41·21
TiO_2	2·43	1·25	0·29	2·16
Al_2O_3	12·25	7·97	23·15	10·89
Cr_2O_3	0·10	0·02	0·07	0·09
FeO*	12·27	8·57	16·20	12·83
MnO	0·14	0·10	0·32	0·12
MgO	12·30	12·78	14·74	12·87
CaO	12·52	16·51	4·75	13·09
Na_2O	1·56	2·52	0·05	1·63
K_2O	0·11	n.a.	0·01	0·11
CO_2	–			5·00
Sum	100·02	99·99	100·24	100·00
Mg#	64·13	72·66	61·86	64·13

*All Fe reported as FeO.
Mg-number = 100 × molar MgO/(MgO+FeO); SLEC1 is the starting composition used in this study; 66039B, cpx and gt represent compositions of base silicate rock, and of constituent clinopyroxene and garnet, respectively; all data were reported originally by Dasgupta *et al.* (2004); n.a., not analysed.

EXPERIMENTAL TECHNIQUES

Starting material

The starting material SLEC1 (Table 1) was prepared by mixing a natural eclogite xenolith powder (66039B; Dasgupta *et al.*, 2004) with reagent grade and natural carbonates (Dasgupta *et al.*, 2004). The silicate fraction (66039B) of our starting material falls along the thermal divide in the Fo–CaTs–Qtz system (at the crossover of CaTs–En and Fo–An; Kogiso *et al.*, 2004*a*) and thus is silica-deficient compared with typical ocean crust. It was selected because its major element composition accounts for plausible subduction zone modification of typical ocean crust (Kogiso *et al.*, 2003; Dasgupta *et al.*, 2004, 2005*a*). CO_2 (5 wt %) was introduced by adding a mixture of natural siderite, magnesite and reagent grade $CaCO_3$, Na_2CO_3, and K_2CO_3 to keep the Ca:Mg:Fe:Na:K unmodified with respect to the base silicate fraction and thus to mimic the process of ocean-floor carbonation (e.g. Alt & Teagle, 1999; Nakamura & Kato, 2004) and possible modification during subduction (Dasgupta *et al.*, 2005*a*, and references therein)

Experimental procedure

All experiments were carried out at 3 GPa using an end-loaded piston-cylinder apparatus, ½ inch assembly with

Table 2: Summary of 3 GPa experiments: run conditions, phase assemblages and phase proportions

Run no.	T (°C)	t (h)	Assemblage	Weight fractions						Σr^2
				Gt	Cpx	Ilm	[Cc-Dol]$_{ss}$	L$_c$	L$_s$	
A435†	*1010*	*164*	*Gt+Cpx+Ilm+[Cc-Dol]$_{ss}$*	*0·39*	*0·47*	*0·04*	*0·10*	–	–	*2·55*
A372†	*1050*	*48*	*Gt+Cpx+Ilm+[Cc-Dol]$_{ss}$*	*0·38*	*0·49*	*0·03*	*0·10*	–	–	*2·83*
A382†	*1075*	*96*	*Gt+Cpx+Ilm+L$_c$*	*0·40*	*0·46*	*0·03*	–	*0·10*	–	*3·02*
A388†	1080	22	Gt+Cpx+Ilm+L$_c$	0·40	0·46	0·03	–	0·11	–	1·02
A380†	*1100*	*24*	*Gt+Cpx+Ilm+L$_c$*	*0·40*	*0·47*	*0·04*	–	*0·09*	–	*1·40*
A373†	1125	25	Gt+Cpx+Ilm+L$_c$	0·40	0·47	0·04	–	0·09	–	1·67
A375†	1150	6	Gt+Cpx+Ilm+L$_c$	0·40	0·48	0·03	–	0·09	–	1·49
A381†	1175	24	Gt+Cpx+Ilm+L$_c$	0·39	0·47	0·04	–	0·10	–	1·24
A410	1225	20·5	Gt+Cpx+Ilm+L$_c$+/Gt+Cpx+L$_c$+L$_s$	0·37	0·46	0·02	–	0·11	0·04	0·80
A413	1275	20	Gt+Cpx+L$_c$+/Gt+Cpx+L$_c$+L$_s$	0·34	0·44	–	–	0·10	0·12	0·25
A418	1315	24	Gt+Cpx+L$_c$+/Gt+Cpx+L$_c$+L$_s$	0·33	0·38	–	–	0·09	0·20	0·40
A423	1350	22	Gt+Cpx+L$_c$+/Gt+Cpx+L$_c$+L$_s$	0·26	0·30	–	–	0·06	0·38	0·09
A429	1375	22	Gt+Cpx+L$_c$+/L$_s$	0·17	0·17	–	–	0·03	0·63	0·10
A426	1400	21	Gt+Cpx+/L$_s$	0·09	0·01	–	–	–	0·89	0·29

Modes are calculated by least-squares regression analyses using all the oxides including CO_2; Σr^2 is the sum of squared residuals and is an indicator of degree of chemical equilibration; phase compositions of the runs reported in italics are from Dasgupta *et al*. (2004); phase assemblage of the runs marked by † are originally from Dasgupta *et al*. (2004); a slash separates assemblages in capsules with two zones. Gt – garnet, Cpx – clinopyroxene, Ilm – ilmenite–geikielite solid solution, [Cc-Dol]$_{ss}$ – calcio-dolomitic solid solution, L$_c$ – carbonate-rich liquid, L$_s$ – silicate-rich liquid.

$BaCO_3$ pressure cell, and Pt–graphite double capsules at the University of Minnesota, following the calibration of Xirouchakis *et al.* (2001) and procedures as described by Dasgupta *et al.* (2004, 2005*a*). After the experiments, capsules were embedded in epoxy, ground longitudinally, and polished to a ¼ μm finish, using diamond pastes, for textural and compositional analyses. Because quenched carbonate melts are delicate and water-soluble, the samples were polished without water.

Analytical techniques

Wavelength-dispersive spectrometry (WDS) point analyses of the resulting phases were performed using a JEOL JXA8900R electron microprobe at the University of Minnesota. Accelerating voltage was set at 15–20 kV for all the phases. Analyses of the silicate and oxide minerals were performed using a fully focused 20 nA beam. Carbonate melts were analysed with a defocused beam of 1–6 μm and a current of 1–3 nA, depending on the dimension of the interstitial quenched melt pool. For runs where immiscible silicate melts did not segregate to form a large melt pool (A413, A418, and A423), a beam diameter of 1–6 μm and a current of 2–5 nA were employed to measure the silicate melts. We attempted to sample clean glass, but when this was not available we used a broad (up to 10 μm) beam to reintegrate quenched melt regions with exsolved Fe–Ti oxides. To obtain a reasonable estimate of the melt compositions from these experiments, we averaged as many spot analyses as possible by repolishing a new surface after each microprobe session for up to two to three times and reanalysing the quenched melt. Relatively large quenched silicate-melt pools for runs A429 and A426 were analysed with a 30 μm, 10 nA beam. Counting times for all elements were 20 s on peak and 10 s on each background for minerals and silicate melts, and 10 s on peak and 5 s on backgrounds for quenched carbonate melt. Analytical standards were natural cpx, garnet, olivine, ilmenite, feldspar, chrome spinel, and natural basalt glass for minerals and quenched silicate glass. For quenched carbonate mats, Ca and Mg were standardized on natural dolomite and Fe on siderite.

To confirm textural interpretations regarding the presence of carbonate and silicate melts, high-resolution imaging of the run products was performed in a JEOL-JSM-6500F field emission gun scanning electron microscope in the IT Characterization Facility of University of Minnesota.

EXPERIMENTAL RESULTS

Experimental conditions and corresponding phase assemblages are listed in Table 2 and micrographs of the run products are presented in Fig. 2. Phase proportions

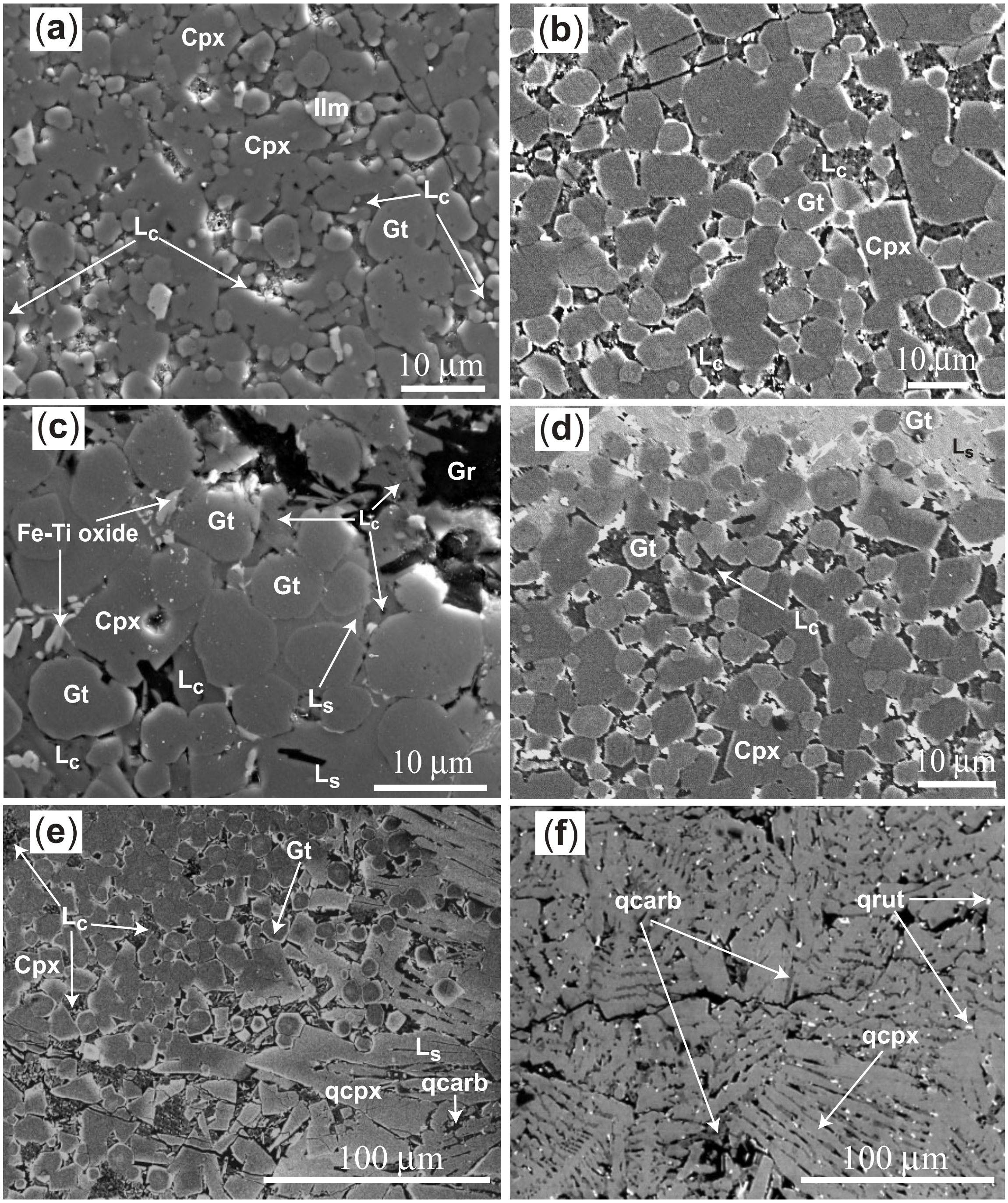

Fig. 2. Secondary electron images from high-resolution field emission gun scanning electron microscope (a and c) and back-scattered electron images from electron microprobe (b, d, e, and f) of experimental charges. (a) Run A375 (3 GPa, 1150 °C, 6 h): carbonate-rich melt (L_c) occurs along grain edges and at triple grain junctions of garnet, cpx, and ilmenite [see also Dasgupta *et al.* (2004, fig. 2b)]. (b) Run A423 (3 GPa, 1350 °C, 22 h): immiscible carbonate-rich (L_c) melts are present at the interstices of garnet and cpx. (c) Run A418 (3 GPa, 1315 °C, 24 h): both carbonate-rich (L_c) and silicate-rich (L_s) melts are present along with residual garnet and cpx. Blebs and stringers of Fe–Ti oxides within domains of silicate-rich melts are interpreted to be quench products. Gr, graphite capsule. (d) Run A423 (3 GPa, 1350 °C, 22 h): coexisting carbonate-rich (L_c) and silicate-rich (L_s) melts are observed as well as residual cpx and garnet. Immiscible silicate-rich melt is concentrated towards the top of the capsule, whereas conjugate carbonate-rich (L_c) melts are confined to interstitial melt pools distributed across the charge. (e) Run A429 (3 GPa, 1375 °C, 22 h): quenched mat of carbonated silicate melt is composed of quenched cpx (qcpx) and quenched carbonate (qcarb). Also shown are residual garnet and cpx with interstitial quenched carbonate melt. (f) Run A426 (3 GPa, 1400 °C, 21 h): a mat of cpx (qcpx), carbonate (qcarb), and rutile (qrut) is interpreted as a quench product of a single melt phase present during the experiment. Residual garnet and minor cpx (not shown) are also present.

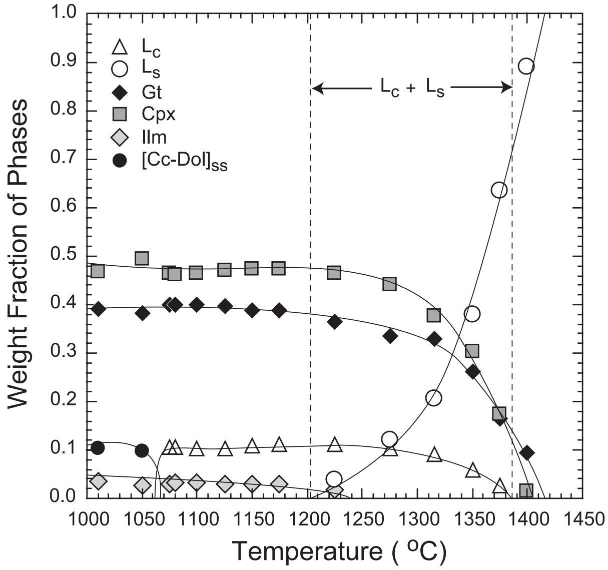

Fig. 3. Modes (expressed as weight fractions) of garnet, cpx, ilmenite, calcio-dolomitic solid solution, carbonatitic melt, and silicate-rich melt from mass-balance calculation of SLEC1 partial melting experiments at 3 GPa. The solidus is between 1050 and 1075 °C and the liquidus is at ~1415 °C. Temperature interval (dashed lines) for coexistence of immiscible carbonate (Lc) and silicate (Ls) melt is also shown. The melting interval of carbonated eclogite SLEC1 is close to 350 °C.

inferred from mass-balance calculations are also given in Table 2 and are plotted in Fig. 3 as a function of temperature. Compositions of minerals and melts are listed in Tables 3–7 and plotted in Figs 4–7.

Phase assemblages and textures

Near solidus phase relations for SLEC1 have been reported by Dasgupta *et al.* (2004). At 3·0 GPa, the subsolidus assemblage (≤1050 °C) consists of garnet, cpx, ilmenite, and calcio-dolomitic solid solution. At higher temperatures, quenched carbonate melts (1075–1375 °C) and silicate melts (1225–1400 °C) are present. Above the solidus, at 1075 °C the appearance of calcio-dolomitic melt coincides with the disappearance of crystalline carbonate. Carbonatitic melt persists with residual garnet, cpx, and ilmenite to at least 1175 °C (Fig. 2a). At 1225 °C, a coexisting silicate glass appears. Ilmenite disappears between 1225 and 1275 °C. Carbonate and silicate melts coexist at least up to 1375 °C (Fig. 2c and d) and at 1400 °C a single CO_2-rich silicate melt is observed (Fig. 2e and f). Garnet and cpx are observed in all experimental charges, but based on phase proportion trends (Fig. 3), cpx is inferred to disappear within 10–20 °C of the liquidus and garnet is inferred to be the remaining phase at the liquidus, which is estimated to be at ~1415 °C.

Quenched carbonate melts consist primarily of feathery mats of dolomite–ankerite$_{ss}$ crystals (see Dasgupta *et al.*, 2004, fig. 2b) and are present at triple grain junctions and along grain edges of residual garnet, cpx, and ilmenite (Fig. 2a). For relatively high-temperature runs (>1225 °C), acicular crystals of quench cpx and needles of rutile are also identified within the interstitial pools of carbonate melts. Immiscible silicate melts quench primarily to glass. However, variable amounts of exsolved Fe–Ti oxide are observed within quenched silicate glass at 1225, 1275, 1315, and 1350 °C (Fig. 2c and d). At 1375 and 1400 °C, the quenched silicate melt is an aggregate of quench-cpx, carbonate and rutile (Fig. 2e and f), and devoid of any glass.

Textural relations do not indicate any definite preferential wetting of mineral grains by carbonate or silicate melts (Fig. 2c and d); however, quench-overgrowths on residual garnet and cpx (Fig. 2b–e) suggest selective wetting of grain edges by silicate melt. In runs A410 (1225 °C), A413 (1275 °C), A418 (1315 °C), and A423 (1350 °C), interstitial silicate melt is observed to be present towards the top of the capsule only, where carbonate melts are confined to interstitial melt pools distributed across the charge (Fig. 2d, Table 2). This also indicates that the silicate melts form an interconnected, permeable, network under conditions where carbonate melt pockets are isolated. In run A429 (1375 °C), complete separation of quenched pools of silicate melt from a zone of garnet + cpx + interstitial carbonate melt is observed (Fig. 2e; Table 2), which further supports our inference of diminished mobility of carbonate melts when silicate melts are present.

Approach to chemical equilibration

The experiments reported here are unreversed and the back-scattered electron images show zoning in garnet for runs up to 1350 °C, reflecting incomplete chemical equilibration. However, an approach to equilibrium can be assessed as follows. All the experiments have been mass-balanced and for 10 new experiments whose phase compositions are reported here for the first time, the average sum of squared residuals (Σr^2) is 0·74. Considering uncertainties in analyses of alkalis and estimation of CO_2 in quenched carbonate melts, these residuals are considered to be acceptable. The average Σr^2 is reduced to 0·50 when Na is left out of the mass-balance calculation. Garnet compositions (rim compositions for runs up to 1350 °C) also show systematic shifts with increasing temperature. Finally, generalized thermometers based on Fe^{2+}–Mg partitioning between garnet and clinopyroxene (Ellis & Green, 1979; Krogh-Ravna, 2000) were compared with known experimental temperatures. Based on average analyses of garnet and clinopyroxenes, calculated temperatures fall within 65 ° of the nominal run temperatures. We consider this result to be supportive, given that average mineral compositions of the charge and not the texturally coexisting garnet–cpx pairs were used.

Table 3: Composition of carbonate-rich melt

Run no.:	A382	A388	A380	A373	A375	A381	A410	A413	A418	A423	A429
T (°C):	1075	1080	1100	1125	1150	1175	1225	1275	1315	1350	1375
n:	4	5	4	6	5	7	10	8	7	5	6
SiO_2	1·88 (29)	1·97 (31)	2·21 (41)	2·31 (53)	2·57 (95)	2·93 (65)	4·01 (71)	4·45 (85)	5 (1)	4·85 (91)	4·88 (85)
TiO_2	0·02 (3)	0·01 (1)	0·01 (2)	0·07 (1)	0·04 (1)	0·08 (8)	0·30 (11)	0·42 (17)	0·51 (25)	0·61 (18)	0·78 (12)
Al_2O_3	0·76 (36)	0·85 (25)	0·79 (31)	0·81 (21)	0·87 (17)	0·92 (31)	1·20 (53)	1·30 (55)	1·37 (39)	1·83 (36)	2·24 (24)
Cr_2O_3	n.a.	0·03 (2)	0·02 (1)	0·07 (2)	0·02 (3)	0·04 (1)	n.a.	n.a.	n.a.	n.a.	n.a.
FeO*	10 (1)	9 (1)	8·81 (97)	8·99 (81)	9·57 (19)	9·73 (41)	12 (2)	12 (2)	14 (1)	15·81 (45)	16·01 (51)
MnO	0·22 (7)	0·83 (21)	0·72 (4)	0·47 (5)	0·04 (5)	0·03 (1)	0·10 (19)	0·52 (23)	0·45 (37)	0·00 (2)	0·26 (4)
MgO	12·20 (53)	11·07 (89)	10·07 (31)	11·04 (33)	10·60 (18)	11·09 (26)	10 (2)	8 (2)	6·65 (48)	6·88 (52)	5·99 (15)
CaO	31·16 (37)	31·18 (75)	31·28 (36)	31·28 (43)	32·49 (56)	32·44 (71)	30 (2)	30 (1)	30 (2)	29 (2)	26 (1)
Na_2O	0·89 (52)	0·91 (34)	1·81 (32)	1·57 (29)	1·56 (21)	1·70 (5)	1·22 (17)	0·54 (24)	0·13 (8)	0·14 (2)	0·27 (6)
K_2O	0·07 (5)	0·18 (7)	0·18 (2)	0·17 (2)	0·08 (2)	0·00 (1)	0·09 (14)	0·04 (7)	0·05 (3)	0·03 (1)	0·07 (2)
Sum	57·22	55·84	56·01	56·80	57·82	58·94	58·55	57·92	57·75	58·74	56·76
CO_2 (by diff.)	42·78	44·17	43·99	43·20	42·20	41·10	41·45	42·08	42·25	41·26	43·24
Na_2O-calc.	7·22	7·19	7·43	7·55	7·22	7·00	6·14	4·51	4·67	4·74	6·77
Mg-no.	68·46	69·13	67·07	68·66	66·39	67·00	60·84	53·85	45·74	43·70	39·99

Errors in parentheses are 1σ of the mean, reported as least units cited; 1·88 (29) should be read as 1·88 ± 0·29 wt %. Errors are reported where 3 or more analyses were available to average. *n*, number of analyses averaged. n.a., not analysed. FeO* indicates all Fe as FeO. CO_2 is calculated from difference of 100 and electron microprobe total. Na_2O-calc. is reconstructed concentration to achieve zero residual for the oxide using the method of Yaxley & Green (1996). Mg-number is molecular Mg/(Mg + Fe) × 100.

Table 4: Composition of silicate-rich melt

Run no.:	A410	A413	A418	A423	A429	A426
T (°C):	1225	1275	1315	1350	1375	1400
n:	11	14	17	13	18	17
SiO_2	33·8 (36)	37·7 (31)	40·9 (25)	41·9 (18)	42·9 (18)	43·3 (14)
TiO_2	19·4 (32)	13·6 (31)	8·6 (21)	5·4 (15)	3·6 (7)	2·6 (3)
Al_2O_3	2·43 (81)	4·80 (68)	6·27 (71)	8·03 (50)	9·16 (53)	10·09 (44)
Cr_2O_3	0·05 (3)	0·07 (5)	n.a.	n.a.	n.a.	n.a.
FeO*	25·6 (30)	21·0 (29)	18·3 (21)	16·5 (6)	15·1 (7)	13·8 (6)
MnO	0·12 (11)	0·40 (16)	0·40 (20)	0·15 (7)	0·20 (10)	0·16 (6)
MgO	8·2 (15)	10·5 (18)	10·8 (11)	11·6 (8)	12·3 (7)	13·54 (36)
CaO	5·1 (11)	8·4 (13)	11·8 (15)	14·0 (9)	14·6 (9)	14·70 (54)
Na_2O	5·1 (10)	3·5 (4)	2·9 (21)	2·4 (3)	2·0 (3)	1·75 (29)
K_2O	0·20 (5)	0·03 (3)	0·03 (2)	0·02 (3)	0·14 (6)	0·13 (2)
Sum	100 (*96·46*)	100 (*94·68*)	100 (*93·67*)	100 (*92·95*)	100 (*93·17*)	100 (*94·45*)
Mg-no.	35·57	46·55	52·13	55·68	59·23	63·51

Concentrations of oxides are reported on a volatile-free basis. Values within parentheses for the sum are averages of measured totals from replicate analyses and the difference between 100% and these values provide an estimate of CO_2 in the melt.

Role of quench modification of partial melt compositions

Formation of overgrowths on residual minerals and consequent modifications of partial melt compositions during quench is a long-standing problem in high-pressure, high-temperature experiments in mafic–ultramafic systems. Observations of variable proportions of quench-rims on cpx and garnets in the present study indicate some

Table 5: Composition of garnet

Run no.:	A435	A372	A382	A388	A380	A373	A375
T (°C):	1010	1050	1075	1080	1100	1125	1150
n:	1	5	14	4	3	7	10
SiO_2	40·44	39·44 (14)	39·73 (19)	40·20 (21)	39·30 (17)	40·23 (40)	40·47 (19)
TiO_2	0·38	0·72 (16)	0·59 (16)	0·61 (11)	0·64 (13)	0·69 (18)	0·98 (16)
Al_2O_3	22·39	21·86 (28)	22·22 (25)	22·30 (44)	21·90 (31)	22·15 (21)	22·30 (25)
Cr_2O_3	0·05	0·05 (3)	0·04 (3)	0·09 (2)	0·09 (1)	0·04 (2)	0·02 (3)
FeO*	17·24	18·35 (26)	17·38 (34)	17·31 (42)	17·05 (29)	16·27 (18)	16·02 (34)
MnO	0·30	0·35 (3)	0·33 (3)	0·40 (19)	0·40 (4)	0·29 (5)	0·31 (3)
MgO	13·26	13·35 (29)	13·62 (42)	13·03 (45)	13·83 (31)	13·00 (33)	13·25 (42)
CaO	5·20	5·89 (25)	5·57 (43)	5·65 (36)	5·86 (36)	6·42 (12)	6·47 (43)
Na_2O	0·02	0·09 (2)	0·33 (31)	0·13 (2)	0·13 (4)	0·15 (6)	0·13 (10)
K_2O	0·03	0·03 (1)	0·02 (1)	0·05 (1)	0·05 (2)	0·03 (2)	0·02 (1)
Sum	99·90	100·13	99·83	99·78	99·26	99·27	99·99
Mg-no.	58·91	56·46	58·28	57·31	59·13	58·76	59·60
End-members							
pyrope	0·494	0·476	0·494	0·482	0·497	0·483	0·490
almandine	0·360	0·367	0·354	0·359	0·343	0·339	0·332
grossular	0·139	0·151	0·145	0·150	0·151	0·172	0·172
spessartine	0·006	0·007	0·007	0·008	0·008	0·006	0·007

Run no.:	A381	A410	A413	A418	A423	A429	A426
T (°C):	1175	1225	1275	1315	1350	1375	1400
n:	13	11	10	13	17	12	11
SiO_2	40·70 (30)	40·21 (51)	40·59 (47)	40·76 (80)	40·19 (91)	40·98 (5)	41·23 (30)
TiO_2	0·99 (18)	1·00 (8)	0·95 (5)	0·86 (14)	0·86 (18)	0·77 (8)	0·44 (4)
Al_2O_3	22·41 (31)	22·43 (34)	22·64 (17)	22·84 (53)	22·82 (36)	22·91 (4)	23·44 (14)
Cr_2O_3	0·03 (1)	0·03 (2)	0·02 (3)	0·04 (2)	0·04 (2)	0·05 (2)	0·08 (1)
FeO*	15·97 (41)	16·23 (56)	16·18 (36)	15·38 (50)	13·87 (25)	12·75 (31)	10·30 (36)
MnO	0·09 (1)	0·28 (2)	0·18 (1)	0·28 (4)	0·27 (2)	0·25 (4)	0·23 (5)
MgO	13·57 (26)	13·51 (49)	13·87 (36)	14·20 (49)	14·76 (52)	16·01 (15)	17·21 (39)
CaO	6·23 (27)	6·20 (31)	6·05 (39)	6·32 (51)	6·32 (17)	6·27 (14)	6·50 (16)
Na_2O	0·16 (5)	0·06 (3)	0·10 (3)	0·10 (6)	0·10 (2)	0·11 (6)	0·07 (3)
K_2O	0·03 (1)	0·02 (2)	0·03 (2)	0·03 (2)	0·02 (1)	0·01 (2)	0·02 (1)
Sum	100·19	99·97	100·61	100·82	99·25	100·12	99·52
Mg-no.	60·23	59·73	60·44	62·20	65·48	69·12	74·88
End-members							
pyrope	0·501	0·497	0·506	0·516	0·542	0·576	0·619
almandine	0·331	0·335	0·331	0·313	0·286	0·257	0·208
grossular	0·165	0·161	0·159	0·165	0·167	0·162	0·168
spessartine	0·002	0·006	0·004	0·006	0·006	0·005	0·005

modifications of interstitial melt compositions that were stable during the experiments. However, we believe that any such effects are minor and that the reported average compositions (Tables 3 and 4) are representative of equilibrium melt compositions because: (1) both silicate and carbonate melts show systematic compositional evolution as a function of temperature (discussed in the 'Phase compositions' section); (2) mass-balance calculations, especially for the silicate melt-present runs, produce satisfactory sum of residuals squares (0·1–0·8); (3) values

Table 6: Composition of clinopyroxene

Run no.:	A435	A372	A382	A388	A380	A373	A375
T (°C):	1010	1050	1075	1080	1100	1125	1150
n:	1	11	7	6	5	7	10
SiO_2	53·80	52·36 (33)	53·23 (43)	53·68 (26)	53·68 (23)	52·43 (33)	52·96 (43)
TiO_2	0·52	0·54 (9)	0·54 (5)	0·55 (6)	0·58 (6)	0·69 (3)	0·77 (5)
Al_2O_3	4·47	4·79 (66)	4·08 (31)	4·16 (31)	4·31 (21)	4·68 (30)	4·89 (31)
Cr_2O_3	0·03	0·02 (2)	0·03 (2)	0·01 (3)	0·01 (2)	0·04 (2)	0·02 (2)
FeO*	7·89	7·98 (42)	7·92 (23)	8·06 (13)	8·16 (14)	8·52 (14)	8·67 (23)
MnO	0·10	0·11 (3)	0·09 (2)	0·01 (3)	0·01 (3)	0·00 (3)	0·13 (2)
MgO	14·72	14·93 (37)	14·94 (38)	14·83 (33)	14·73 (33)	14·86 (31)	14·76 (38)
CaO	17·18	16·70 (58)	17·22 (42)	17·00 (34)	17·00 (44)	16·29 (62)	16·11 (42)
Na_2O	2·41	2·08 (16)	1·74 (12)	1·73 (6)	1·71 (6)	1·69 (6)	1·67 (12)
K_2O	0·03	0·02 (1)	0·00	0·02 (1)	0·00 (1)	0·01 (1)	0·03 (1)
Sum	101·14	99·53	99·79	100·05	100·19	99·22	100·00
Mg-no.	76·89	76·93	77·08	76·64	76·29	75·66	75·23

Run:	A381	A410	A413	A418	A423	A429	A426
T (°C):	1175	1225	1275	1315	1350	1375	1400
n:	15	10	13	13	19	14	6
SiO_2	53·11 (13)	52·95 (30)	51·69 (40)	51·51 (42)	51·81 (23)	51·53 (19)	51·52 (13)
TiO_2	0·86 (7)	0·89 (7)	0·81 (6)	0·77 (4)	0·61 (4)	0·53 (5)	0·36 (3)
Al_2O_3	5·03 (21)	5·32 (21)	5·81 (17)	6·28 (30)	6·51 (18)	6·71 (19)	6·94 (11)
Cr_2O_3	0·01 (1)	0·01 (1)	0·04 (3)	0·01 (2)	0·01 (2)	0·02 (2)	0·03 (3)
FeO*	8·87 (32)	8·49 (38)	8·60 (14)	8·31 (32)	7·97 (20)	7·41 (26)	6·15 (17)
MnO	0·20 (2)	0·11 (3)	0·11 (2)	0·12 (3)	0·12 (3)	0·12 (3)	0·11 (2)
MgO	14·66 (26)	14·57 (31)	14·51 (64)	14·54 (80)	15·09 (26)	15·78 (26)	16·60 (33)
CaO	15·98 (32)	16·13 (62)	15·83 (24)	16·01 (87)	15·97 (44)	15·99 (60)	16·21 (32)
Na_2O	1·65 (6)	1·66 (8)	1·61 (6)	1·56 (10)	1·49 (6)	1·33 (6)	1·23 (4)
K_2O	0·04 (1)	0·03 (1)	0·03 (2)	0·03 (1)	0·02 (2)	0·03 (2)	0·03 (1)
Sum	100·39	100·17	99·05	99·14	99·60	99·44	99·17
Mg-no.	74·66	75·36	75·06	75·72	77·16	79·14	82·80

of garnet–silicate melt and cpx–silicate melt Fe*–Mg K_D values show excellent agreement with those obtained from existing partial melting experiments of eclogite or garnet pyroxenite (e.g. Yaxley & Green, 1998; Hirschmann *et al.*, 2003; Kogiso *et al.*, 2003; Pertermann & Hirschmann, 2003*a*). Also, Fe*–Mg K_D values for garnet–carbonate melt and cpx–carbonate melt are similar to those observed by Yaxley & Brey (2004) between 3·0 and 3·5 GPa.

Phase compositions

In the following section we summarize the compositional evolution of five phases observed—carbonate melt, silicate melt, garnet, cpx, and ilmenite—as a function of temperature across the 3 GPa melting interval of SLEC1. The composition of subsolidus crystalline carbonate has been given by Dasgupta *et al.* (2004, 2005*a*) and is not repeated here.

Carbonate melt

Quenched carbonate melts are broadly calcio-dolomitic, with Ca-numbers [molar Ca/(Ca + Mg + Fe)] ranging from 0·60 to 0·55, and show systematic compositional variations throughout the melting interval of SLEC1 at 3 GPa (Table 3, Fig. 4). With increasing temperature from 1075 to 1375 °C, SiO_2 increases gradually from ~2 to 5 wt %. From 1075 to 1175 °C, concentrations of Al_2O_3, TiO_2, FeO*, CaO and MgO, and Mg-number shows little variation. With the appearance of silicate-rich

Table 7: Composition of ilmenite

Run no.:	A435	A372	A382	A388	A380	A373	A375	A381	A410
T (°C):	1010	1050	1075	1080	1100	1125	1150	1175	1225
n:	2	3	1	4	2	7	9	8	3
SiO_2	0·12	0·20 (8)	0·26	0·34 (12)	0·34	0·24 (9)	0·27 (10)	0·14 (5)	0·16 (3)
TiO_2	53·89	50·67 (17)	49·95	51·70 (52)	49·70	52·91 (45)	52·94 (41)	52·74 (34)	56·19 (21)
Al_2O_3	0·32	0·50 (3)	0·75	0·93 (34)	0·93	0·42 (11)	0·23 (7)	0·03 (2)	0·89 (23)
Cr_2O_3	0·04	0·05 (1)	0·06	0·01 (2)	0·00	0·05 (3)	0·02 (2)	0·02 (1)	0·02 (1)
FeO*	39·03	40·45 (19)	41·29	39·57 (32)	40·57	39·51 (31)	39·55 (19)	39·15 (15)	31·43 (22)
MnO	0·12	0·18 (4)	0·15	0·21 (7)	0·33	0·17 (5)	0·14 (6)	0·17 (3)	0·18 (7)
MgO	6·12	7·28 (22)	6·70	6·05 (12)	6·25	6·04 (11)	6·06 (4)	6·26 (11)	10·76 (36)
CaO	0·43	0·60 (7)	0·68	0·93 (5)	0·96	0·73 (13)	0·72 (10)	0·32 (12)	0·77 (19)
Na_2O	0·01	0·02 (3)	0·13	0·37 (11)	0·37	0·12 (3)	0·06 (2)	0·06 (4)	0·06 (2)
K_2O	0·00	0·04 (3)	0·04	0·00	0·00	0·00	0·00	0·00	0·00
Sum	100·08	99·99	100·00	99·90	99·13	100·20	100·03	98·90	100·47
Mg-no.	21·84	24·29	22·42	21·42	21·54	21·41	21·47	22·18	37·90

melt at ≥1200 °C, there are noticeable changes in most of the major element oxide vs temperature trends. With increasing temperature from 1225 to 1375 °C, carbonate melts become richer in Al_2O_3, TiO_2 and FeO*, and poorer in MgO and CaO. Mg-numbers of immiscible carbonate melts diminish with temperature.

The low measured concentrations of Na_2O in the carbonate melts (∼0·3–1·8 wt %) are probably artefacts of polishing damage, as mass-balance calculations indicate deficits of the same. Reconstruction of the carbonate melt compositions, using mass balance to achieve zero residuals for Na_2O (Yaxley & Green, 1996) indicates that the carbonate melts are Na_2O-rich, with concentrations ranging between ∼4·5 and 8 wt % (Table 3).

Silicate melt

Low microprobe (93–96·5 wt %) totals in replicate analyses of quenched silicate melts indicate that SLEC1-derived partial silicate melts contain ∼3·5–7·0 wt % dissolved CO_2 (Table 4). Inferred CO_2 concentrations in the silicate melt increase from ∼3·5 ± 2·5 wt % at 1225 °C to ∼7·0 ± 1·75 wt % at 1350 °C, and then decrease to ∼5·5 ± 0·4 wt % at 1400 °C as the melt composition approaches the bulk composition of SLEC1 (5 wt % CO_2; Fig. 5). Inferred CO_2 concentrations are at the low end of solubilities measured in high-pressure experiments in natural and synthetic silicate systems (Brey & Green, 1976; Eggler & Mysen, 1976; Blank & Brooker, 1994; Thibault & Holloway, 1994; Brooker *et al*., 2001). They are lower than predicted from the 2 GPa solubility parameterization of Brooker *et al.* (2001). This is as expected from melts in equilibrium with carbonate melt, rather than CO_2 vapor. To facilitate comparison between analyses of silicate melts and those from other experiments or natural lavas, all the major element oxide concentrations of silicate melts discussed below, and presented in Table 4 and Fig. 5, are recalculated to microprobe totals of 100%.

Silicate partial melts of SLEC1 vary from melilitites at lower temperature to melilite nephelinites (Le Bas, 1989) at higher melt fractions. SiO_2 increases from 33·8 wt % at 1225 °C to 42·9 wt % at 1375 °C. The melt at 1400 °C has 43·3 wt % SiO_2 and approaches the composition of the starting material. From 1225 to 1400 °C Al_2O_3, MgO, CaO, and Mg-number show gradual increases, whereas TiO_2, FeO*, and Na_2O show steady decreases with rising temperature and increasing melt fraction (Table 4, Fig. 5). The most interesting compositional features of the immiscible silicate partial melts are their extreme enrichments of TiO_2 and FeO*, particularly at lower temperatures. At 1225 °C the silicate melt has ∼19 wt % TiO_2 and ∼25 wt % FeO*. With increasing temperature and melt fractions, both TiO_2 and FeO* diminish dramatically and approach the starting material concentrations for the respective oxides (Fig. 5).

Garnet

Garnet compositions are given in Table 5 and plotted in Fig. 6. Several oxides, including TiO_2, FeO* and MgO, and Mg-number, show kinks in their trends around 1225 °C, the temperature of first appearance of immiscible silicate melt and of ilmenite breakdown. The Mg-number remains ∼60 from the solidus to 1225 °C and then increases smoothly to ∼75 at 1400 °C. With

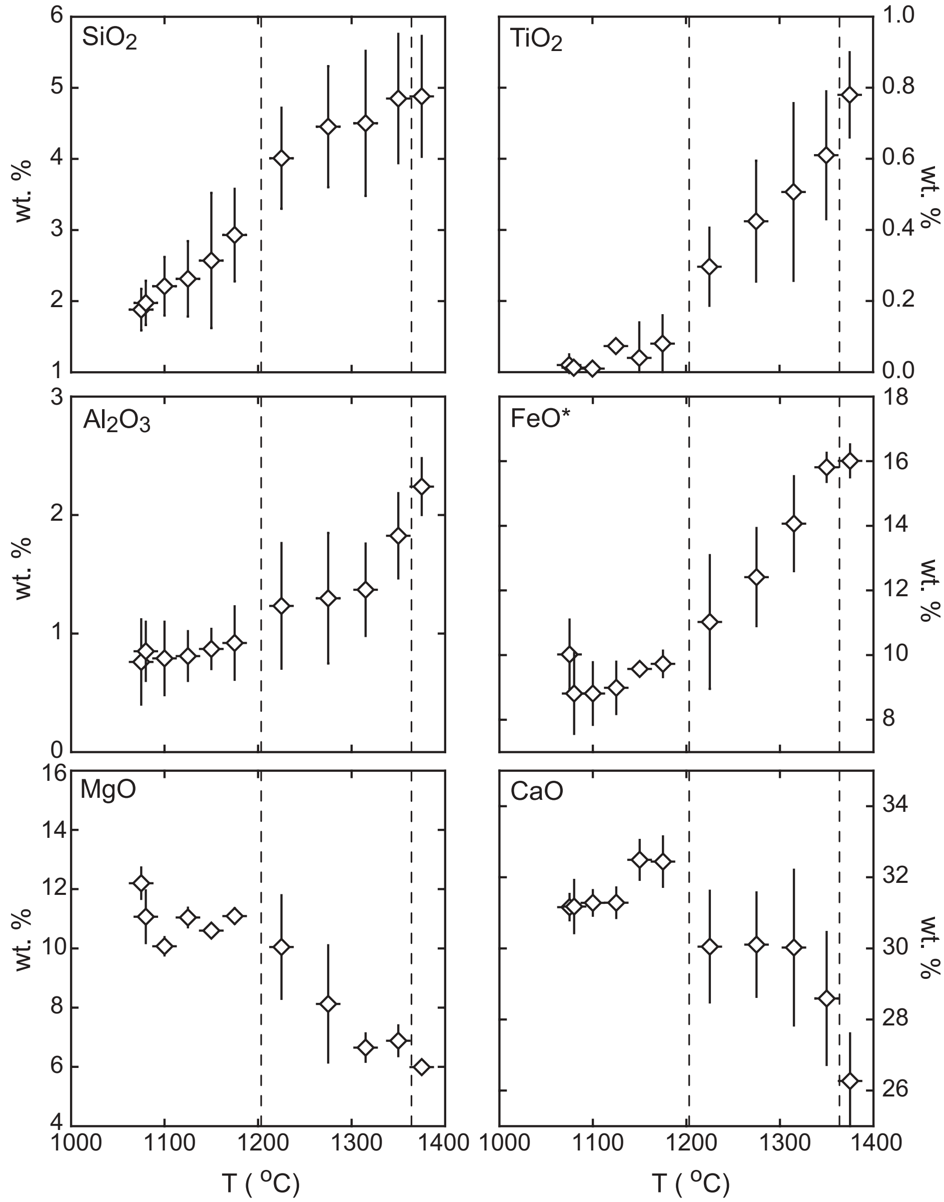

Fig. 4. Compositions of carbonate-rich partial melts from SLEC1 partial melting experiments. Error bars are ±12 °C and ±1σ (wt %). Two melts are stable in the temperature interval between the two vertical dashed lines. A definite change in carbonate melt composition can be noted from the change of slope in the oxide (wt %) vs temperature trends with the appearance of immiscible silicate melt.

increasing temperature, TiO_2 contents increase from ~0·6 to ~1·0 wt %, while ilmenite is present, but are then reduced with increased melting and temperature to ~0·4 wt % at 1400 °C.

Clinopyroxene

Compositions of aluminous clinopyroxene vary systematically across the melting interval of SLEC1 at 3 GPa (Table 6, Fig. 7). From the solidus (1050–1075 °C) to 1175 °C, their Mg-numbers vary little, from ~77 to ~75, but following the onset of silicate melting at 1225 °C, they increase steadily to ~83 at 1400 °C. Al_2O_3 concentrations increase steadily from ~4 wt % at the solidus to ~7 wt % at 1400 °C; TiO_2 increases from ~0·5 at the solidus to ~0·9 at 1175 °C, but then decreases steadily, after the elimination of ilmenite from the residue, with increased degree of silicate melting, to ~0·4 just below the liquidus. Na_2O concentrations drop from 2·1 wt % to ~1·7 wt % across the solidus and then stay near-constant up to 1175 °C. From 1225 °C to 1400 °C, Na_2O drops from ~1·7 to 1·0 wt % as the silicate melt fraction increases.

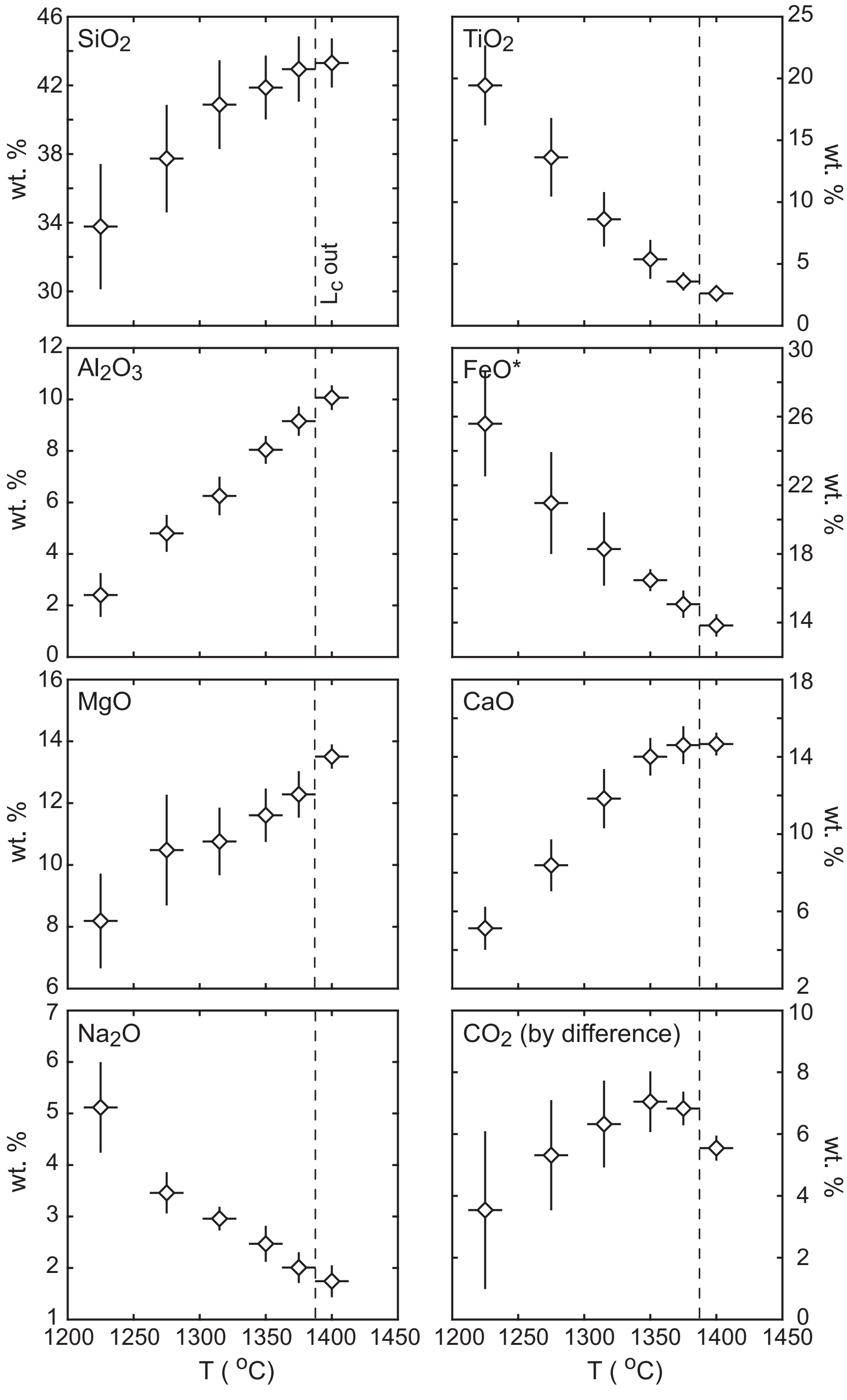

Fig. 5. Compositions of silicate-rich partial melts from SLEC1 partial melting experiments. Concentrations of SiO_2, TiO_2, Al_2O_3, FeO*, MgO, CaO, and Na_2O are plotted on a volatile-free basis, and that of CO_2 is by difference of the average electron microprobe total from replicate analyses and 100%. Error bars are ±12 °C and ±1σ (wt %).

Ilmenite

At 3 GPa, the accessory Fe–Ti oxide phase in the melting interval of SLEC1 is stoichiometric ilmenite–geikielite solid solution (Table 7). From below the solidus (≤1050 °C) to 1175 °C, ilmenite composition varies little, with MgO concentrations of 6–7 wt % (Mg-number of ~21–22). At 1225 °C, with the appearance of Fe–Ti-rich silicate melt, the MgO content of ilmenite increases

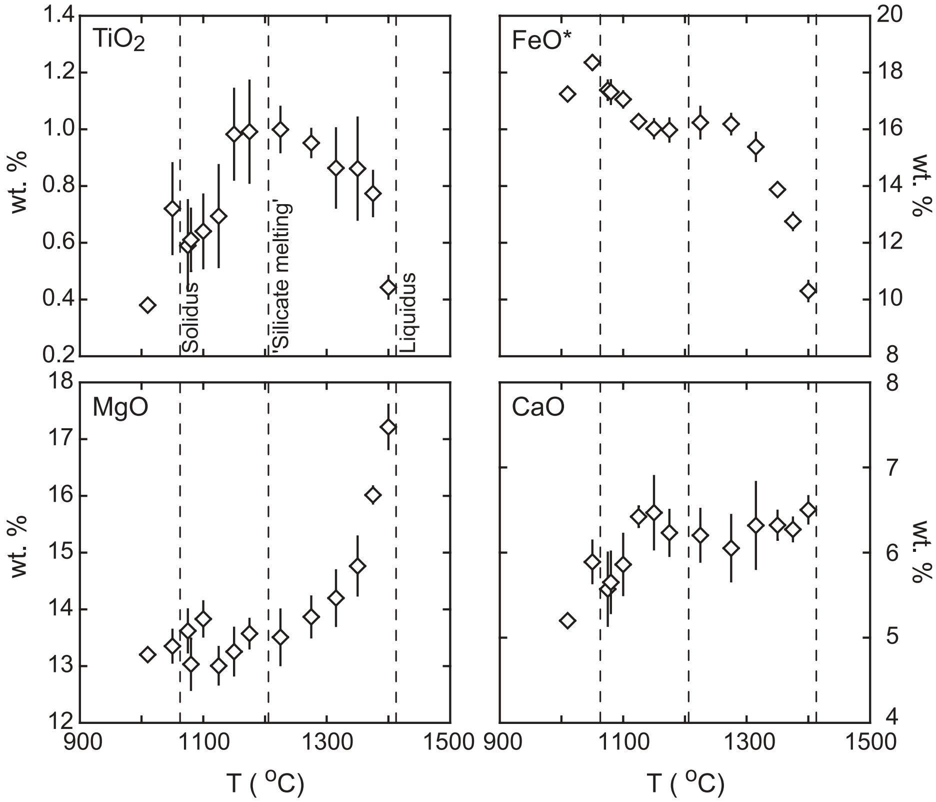

Fig. 6. Compositions of garnet from SLEC1 partial melting experiments. Error bars are $\pm 12\,^{\circ}C$ and $\pm 1\sigma$ (wt %). The absence of an oxide error bar for the 1010 °C data points indicates that fewer than three data points were available to average. Three dashed vertical lines mark the temperature of the solidus, initiation of silicate melt formation, and the liquidus. (Note the relatively small variation of CaO and TiO_2, whereas Mg-number increases with rising temperature as evidenced by increasing MgO and decreasing FeO* after the silicate-rich melts appear.)

sharply to ~11 wt % (Mg-number of ~38). Ilmenite is absent at or above 1275 °C.

DISCUSSION

Carbonate–silicate melt immiscibility during partial melting of carbonated eclogite

Our experiments provide clear evidence for coexisting carbonate and silicate liquids in the melting interval of SLEC1 carbonated eclogite at 3 GPa. This interpretation is supported both by textural evidence and by the compositions of coexisting liquids. The compositional evidence includes noticeable changes in the temperature vs major element oxide trend for carbonate melt at the appearance of immiscible silicate melt in SLEC1 (Fig. 4), and systematic shifts in Fe*–Mg exchange equilibria between the two melts (discussed below). More generally, the relationship between the compositions of these coexisting melts can be illustrated in the temperature vs molar Ca/(Ca + Si) and molar Mg/(Mg + Ti) diagrams shown in Fig. 8. These clearly demonstrate the presence of a miscibility gap between the two conjugate melts in $T-X$ ($CaO-SiO_2$ and $MgO-TiO_2$) space. The shape of the miscibility gap as observed in Fig. 8 probably indicates changes in structure of the silicate melts with increasing temperature. High initial TiO_2 contents indicate a polymerized melt structure with TiO_2 acting as a network-forming species (e.g. Dickinson & Hess, 1985). With rising temperature, the TiO_2 concentration in the silicate melts diminishes rapidly, accompanied by increasing SiO_2. An increase in CaO and Ca/Si, and decrease in Si/Al with increasing temperature probably enhances CO_3^{2-} solubility in the melt (e.g. Kubicki & Stolper, 1995; Dixon, 1997; Brooker *et al.*, 1999, 2001), as the silicate melts become less polymerized and approach the composition of the carbonate melt. The eclogite-derived carbonate-rich melt, in contrast, shows relatively limited compositional evolution as a function of temperature (Fig. 8), indicating very low solubility of SiO_2, TiO_2, and Al_2O_3 in its largely ionic structure.

The well-defined temperature interval of coexisting carbonate and silicate partial melts for carbonated eclogite SLEC1 at 3 GPa is distinct from the behavior observed in carbonated peridotite (Hirose, 1997; Moore & Wood, 1998). At 3 GPa, partial melting

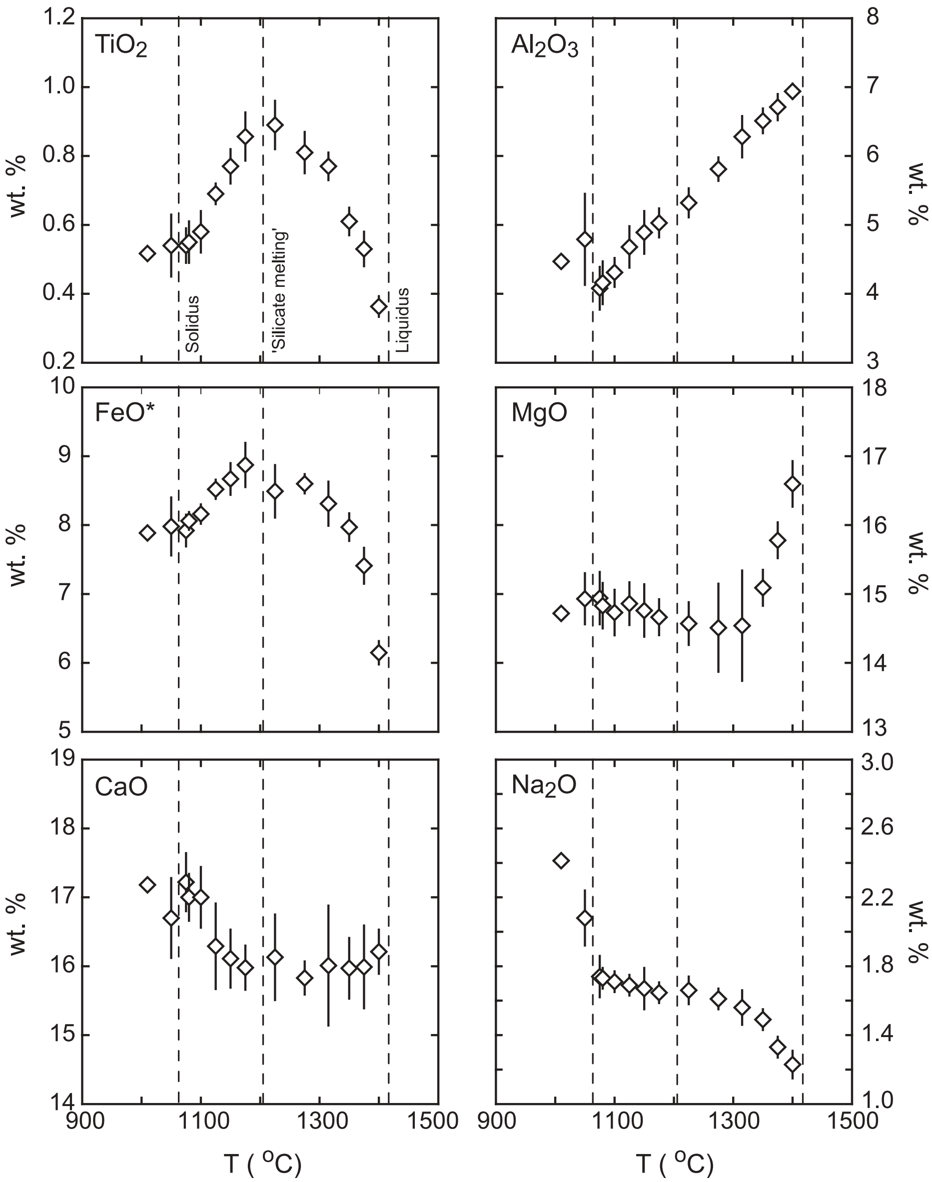

Fig. 7. Compositions of clinopyroxene from SLEC1 partial melting experiments. Error bars are ±12 °C and ±1σ (wt %). The absence of oxide error bars for the 1010 °C data points indicates that fewer than three data points were available to average. Three dashed vertical lines mark the temperature of the solidus, initiation of silicate melt formation, and the liquidus.

experiments with fertile natural peridotite KLB-1 + 5% magnesite (Hirose, 1997) and with model CMS–CO_2 lherzolite (Moore & Wood, 1998) indicate a continuous transition from carbonatite partial melts near the solidus to silica-undersaturated silicate melts at higher temperatures. A continuous transition is also observed at 3·2–8·0 GPa in model CMAS–CO_2 peridotite (Dalton & Presnall, 1998; Gudfinnsson & Presnall, 2005). The difference between the 3 GPa carbonated peridotite studies and our results for carbonated eclogite probably lies in the temperature at which silicate melt is first stabilized. This is illustrated in Fig. 8, which shows that the temperature maximum of the miscibility gap observed for SLEC1 occurs at ~1400 °C. Carbonated peridotite studies (e.g. Hirose, 1997) encountered silicate melt only at temperatures above this miscibility gap, thereby allowing a continuous transition from carbonatite to silicate partial melts. We note the Ca/(Ca + Si)–T and Mg/(Mg + Ti)–T projections of the miscibility gap do not rule out a narrow interval of coexisting carbonatitic and melilititic melts for the study of Hirose (1997) below 1400 °C (Fig. 8).

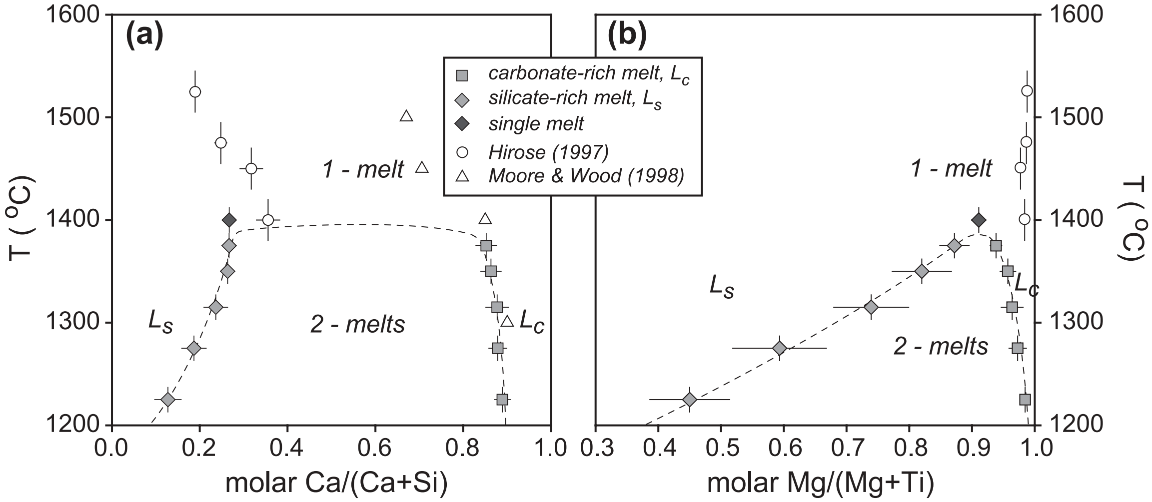

Fig. 8. Temperature–composition diagram showing the miscibility gap between carbonate-rich and silicate-rich conjugate melts with respect to molar CaO/(CaO + SiO_2) (a) and molar MgO/(MgO + TiO_2) (b). The field boundary between one- and two-liquid fields is hand drawn and is not rigorously fitted. Closure of the miscibility gap from these $T{-}X$ diagrams is consistent with textural evidence for the existence of two liquids at 1375 °C and one liquid (dark gray diamond) at 1400 °C. Experimental partial melt compositions from model (CMS–CO_2, Moore & Wood, 1998) and natural (Hirose, 1997) lherzolite + CO_2 systems are also included for comparison. The temperature for 'silicate melting' of carbonated peridotite is apparently too high to intersect the carbonate–silicate two-liquid field at 3 GPa. The molar ratios of melts from this study are calculated using Monte Carlo simulations where the microprobe error (1σ) of individual oxide concentrations from replicate analyses was randomly distributed about the average composition to generate 1000 solutions to the matrix equation; the plotted values and the corresponding error bars are the mean and 1 SD from the generated solution population.

The intersection of melt compositions with the silicate–carbonate miscibility gap in the melting interval of eclogite but not peridotite at 3 GPa presumably relates to the lower temperature of silicate melting for eclogite (e.g. Kogiso *et al.*, 2004*a*). According to Kogiso *et al.* (2004*a*), the chief factors that allow eclogites and pyroxenites to have lower solidi than peridotite are lower Mg-numbers and higher alkali content. Our observations for SLEC1 also suggest that bulk compositions with residual rutile or ilmenite should also stabilize silicate melts at low temperature owing to high activities of TiO_2 and associated TiO_2 enrichments in near-solidus partial melts. Interestingly, Hammouda (2003) also reported immiscible coexisting carbonate and silicate melt for a Ti-free carbonated eclogite bulk composition at 6·0 GPa and 1300 °C, which suggests that other compositional parameters may also play a role in the stability of silicate-rich melts of eclogite at relatively lower temperatures. We believe, however, that at high pressure, the partial melting behavior of carbonated eclogite may be more similar to that of carbonated peridotite, with a gradual transition from carbonate-rich to silicate liquid compositions and without clear immiscibility. This is because we expect the temperature of first appearance of silicate melt to increase with increasing pressure whereas the region of carbonate–silicate melt immiscibility should diminish, owing to increasing solubility of CO_2 in silicate melt.

Isobaric melting phase relation of carbonated eclogite

Melting reactions

Applying the method of Walter *et al.* (1995) yields the following average melting reactions (in weight fractions) for the melting interval of SLEC1:

$$0{\cdot}08\ \text{cpx} + 0{\cdot}90\ [\text{cc--dol}]_{ss} + 0{\cdot}02\ \text{ilm} = 1{\cdot}00\ \text{carb-melt (solidus to } [\text{cc--dol}]_{ss}\text{-out)} \tag{1}$$

$$0{\cdot}25\ \text{cpx} + 0{\cdot}42\ \text{gt} + 0{\cdot}08\ \text{carb-melt} + 0{\cdot}24\ \text{ilm} = 1{\cdot}00\ \text{sil-melt (}[\text{cc--dol}]_{ss}\text{-out to ilm-out)} \tag{2}$$

$$0{\cdot}56\ \text{cpx} + 0{\cdot}31\ \text{gt} + 0{\cdot}13\ \text{carb-melt} = 1{\cdot}00\ \text{sil-melt (ilm-out to carb-melt-out).} \tag{3}$$

Equation (1) indicates that the principal phase contributing to the near-solidus carbonatitic melt is $[\text{cc–dol}]_{ss}$, with minor contributions from cpx and ilmenite. The fraction of carbonate melt changes little from the solidus until silicate melt appears, at which point the carbonate melt fraction is reduced as indicated by reaction (2). Of course, most of the mass of the silicate melt derives also from the silicate and oxide minerals, with a significant contribution of ilmenite (0·24 weight fraction), as required by the TiO_2-rich composition of the melts, and garnet. With increasing melt fraction, the garnet contribution diminishes and the cpx mode entering the

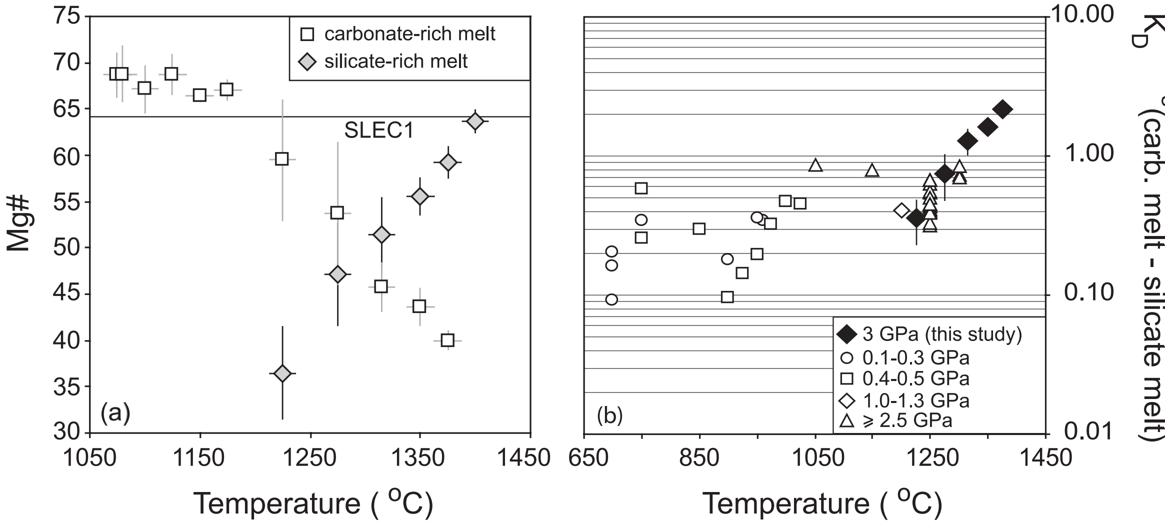

Fig. 9. Variation of Mg-number for carbonate-rich and silicate-rich melts (a) and Fe*–Mg K_D between carbonate and silicate melts (b) as a function of temperature from the partial melting experiments of SLEC1. Fe*–Mg K_D values from other experimental studies on carbonate–silicate immiscibility are also included in (b) for comparison. Other data on carbonate melt–silicate melt immiscibility are grouped according to the nominal pressures of the experiments: 0·1–0·3 GPa, Kjarsgaard *et al.* (1995) and Kjarsgaard (1998); 0·4–0·5 GPa, Kjarsgaard *et al.* (1995) and Kjarsgaard (1998); 1·0–1·3 GPa, Lee & Wyllie (1997); ≥2 GPa, Baker & Wyllie (1990), Lee & Wyllie (1997), Brooker (1998) and Hammouda (2003). The error bars for Mg-number and Fe*–Mg K_D are calculated using Monte Carlo simulation as described in the caption of Fig. 8. The errors for K_D values from the present study are within the size of the symbols where error bars are not shown. Fe*–Mg K_D between immiscible carbonate and silicate melt increases broadly with pressure and temperature.

silicate melt phase increases. Also, as more CO_2 is dissolved into the silicate melt, the fraction of immiscible carbonatitic melt gradually decreases and finally disappears at 1400 °C.

Solidus and liquidus temperatures—effect of carbonates

The solidus (1050–1075 °C) temperature observed for carbonate-bearing composition SLEC1 at 3 GPa is distinctly lower than that observed for comparable compositions of nominally volatile-free pyroxenite, which have solidus temperatures in the range of 1300–1500 °C (see Kogiso *et al.*, 2004*a*, fig. 5). The liquidus (~1415 °C) of carbonated SLEC1 is also slightly lower than for nominally volatile-free equivalent compositions (1450–1550 °C; Kogiso *et al.*, 2004*a*, fig. 6). Because addition of carbonate has a larger effect on the solidus than on the liquidus, it also has the effect of increasing the eclogite-melting interval.

Expansion of the melting interval for carbonated eclogite is partly due to the very low temperature onset of carbonatite melt formation. However, the interval of silicate melt formation is also increased, as carbonated silicate melt appears at ~1200 °C, more than 100 °C lower than silicate melt would be expected in nominally volatile-free eclogites and pyroxenites (Kogiso *et al.*, 2004*a*, and references therein). A similar lowering of the temperature of initial silicate melt formation is observed for carbonated peridotite at 3 GPa; i.e. in experiments with KLB-1 + 5% magnesite, Hirose (1997) observed silicate melts at 1400 °C, whereas the CO_2-free solidus for KLB-1 is near 1500 °C (Takahashi, 1986). With increasing pressure and consequent enhanced solubility of carbonate in silicate melts, carbonate may have a more pronounced effect on the temperature of first-silicate melt appearance. Thus, at 6 GPa, the first silicate melt production for the CMAS lherzolite occurs at ~1875 °C (Presnall *et al.*, 2002, and references therein), whereas 'silicate melt' (>20 wt % SiO_2 in the melt) in CMAS–CO_2 occurs at temperatures as low as 1405 °C (Dalton & Presnall, 1998). Thus, the effects of carbonate on partial melting of upwelling mantle are twofold: in addition to producing carbonatite melts at great depth, more extensive carbonated silicate melt formation commences at depths considerably greater than the volatile-free silicate solidus.

Fe–Mg partitioning between immiscible silicate melts, carbonate melts, cpx and garnet*

The Fe–Mg compositions of coexisting carbonate and silicate liquids in our experiments show systematic variations (Fig. 9). With increasing temperature, Mg-numbers of carbonatite liquids (L_c) diminish whereas those of conjugate silicate liquids (L_s) increase (Fig. 9a). This is due to the marked temperature dependence of the Fe*–Mg partitioning between garnet, cpx, and the two melts, with $K_{DFe^*-Mg}^{cpx-Lc}$, $K_{DFe^*-Mg}^{gt-Lc}$ decreasing with temperature (from ~0·7 to 0·2 and from ~1·3 to 0·3, respectively, from 1175 to 1375 °C) and $K_{DFe^*-Mg}^{cpx-Ls}$,

$K^{gt-Ls}_{DFe^*-Mg}$ increasing with temperature (from 0·2 to 0·4 and from 0·4 to ~0·7, respectively, from 1225 to 1375 °C). The resulting temperature dependence of K_D (Fe*–Mg) between carbonate and silicate melt, shown in Fig. 9b, is similar to that documented from studies of carbonate melt–silicate melt immiscibility at 2–3 GPa (Baker & Wyllie, 1990; Lee & Wyllie, 1997; Brooker, 1998). When compared with data from a wider range of pressures, it is also apparent that there could be a pressure dependence for the K_D (Fig. 9b), with Fe^{2+} partitioning preferentially into carbonate melt at higher pressures. When immiscible silicate melt is not present, modest decreases of $K^{gt-Lc}_{DFe^*-Mg}$ with increasing temperature (from ~1·7 to ~1·4 from 1075 to 1175 °C) are also observed. Yaxley & Brey (2004) also found diminishing $K^{gt-Lc}_{DFe^*-Mg}$, from ~1·7 at 1180 °C to ~1·2 at 1250 °C, in 3 GPa experiments on carbonated eclogite. On the other hand, in the absence of immiscible silicate melt, $K^{cpx-Lc}_{DFe^*-Mg}$ shows little variation (~0·65–0·70) between 1075 and 1175 °C and is similar to values reported by Yaxley & Brey (2004) (0·8 at 1180 °C and 0·6 at 1250 °C).

Partitioning of Ti between coexisting phases during melting of carbonated eclogite

An interesting feature of the silicate partial melts of SLEC1 is the very high TiO_2 concentrations (up to ~19·4 wt % TiO_2) derived from a bulk composition with modest total TiO_2 (2·16 wt %). To our knowledge, similarly TiO_2-rich melts have not been observed previously in partial melting experiments involving mafic or ultramafic lithologies. The cause of these enrichments must be related to low values of mineral–melt partition coefficients for Ti. In this section we discuss Ti partitioning between silicate partial melts of SLEC1 and cpx, garnet and carbonate-rich melt and evaluate them in the light of previous studies of silicate melt–garnet–cpx equilibria.

Both D^{cpx-Ls}_{Ti} and D^{gt-Ls}_{Ti} from the present study depend strongly on temperature. D^{cpx-Ls}_{Ti} diminishes from 0·15 ± 0·02 at 1400 °C to 0·05 ± 0·01 at 1225 °C; D^{gt-Ls}_{Ti} diminishes from ~0·2 ± 0·04 to 0·05 ± 0·01 over the same interval. Thus, strong enrichments in TiO_2 may be related in part to stabilization of melt at low temperature. On the other hand, Pertermann & Hirschmann (2003*a*) noted trends of increasing D^{cpx-Ls}_{Ti} and D^{gt-Ls}_{Ti} with decreasing temperature from a compilation of experimental partial melting studies of pyroxenites and peridotites. Consequently, the observed low values of D^{cpx-Ls}_{Ti} and D^{gt-Ls}_{Ti} in our experiments cannot be caused by low temperature alone.

Another factor that may diminish D^{cpx-Ls}_{Ti} and D^{gt-Ls}_{Ti} is TiO_2 enrichment in the liquid (Fig. 10). For example, in experiments in Ti-rich systems, low values of D^{gt-Ls}_{Ti} and D^{cpx-Ls}_{Ti} are observed (Van Orman & Grove, 2000; Dwarzski & Draper, 2004; R. E. Dwarzski, personal communication, 2005) (Fig. 10). Similar decreases of D_{Ti} with TiO_2 concentration in the melt are observed for opx–silicate melt equilibria (Xirouchakis *et al.*, 2001). This non-Henrian behavior of TiO_2 in silicate melts is probably a contributing factor to the large TiO_2 enrichments observed in the silicate partial melts from our experiments. However, it would be circular reasoning to conclude that TiO_2-rich melts are both the principal cause and an effect of low D_{Ti}. Other influences must also be considered.

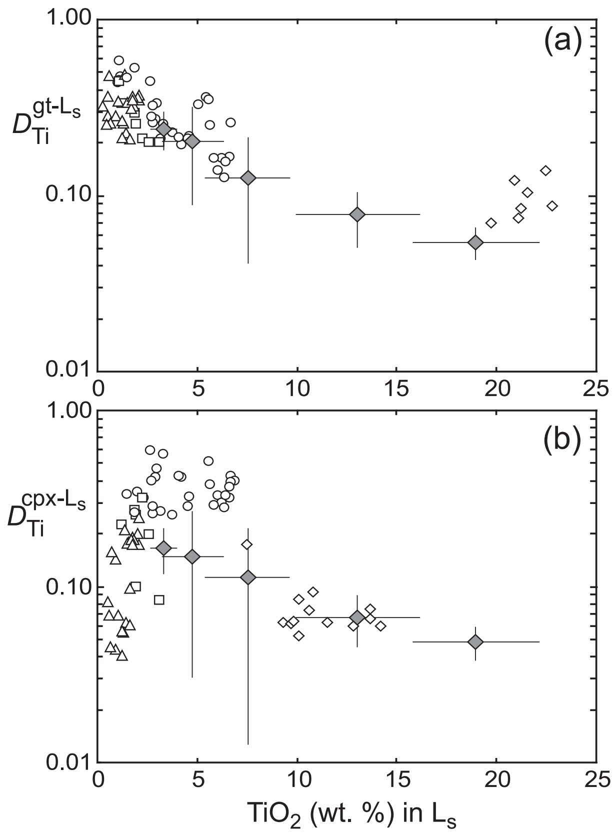

Fig. 10. Plot of TiO_2 partition coefficients (grey diamonds) between garnet and silicate-rich melt (a), cpx and silicate-rich melt (b) as a function of TiO_2 concentration (wt %) in silicate melts. Also shown for comparison are partition coefficients from high-pressure partial melting experiments on peridotitic assemblage (△, Walter, 1998; Longhi, 2002), MORB-like eclogite assemblage (○, Yaxley & Green, 1998; Pertermann & Hirschmann, 2002, 2003*a*; Pertermann *et al.*, 2004), silica-deficient garnet pyroxenite assemblage (□, Hirschmann *et al.*, 2003; Kogiso *et al.*, 2003), and experiments in Ti-rich systems in relation with lunar basalt petrogenesis [◇, Van Orman & Grove (2000) for cpx–melt; Dwarzski & Draper (2004) and R. E. Dwarzski (personal communication, 2005) for garnet–melt]. The D values from this study are calculated using Monte Carlo simulations where the microprobe error (1σ) of TiO_2 concentrations from replicate analyses of both crystals and melts was randomly distributed about the average composition of TiO_2 to generate 1000 solutions to the matrix equation; the plotted values and the corresponding error bars are the mean and 1 SD from the generated solution population.

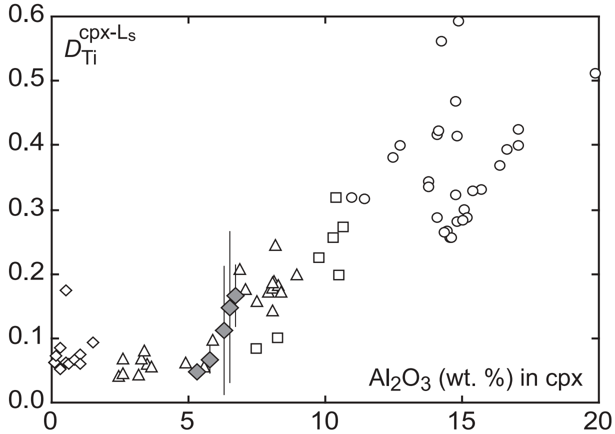

Fig. 11. Partition coefficients for TiO_2 between cpx and silicate-rich melts as a function of the Al_2O_3 content of cpx. The strong positive correlation suggests that aluminium enrichment in cpx enhances the stability of Ti in cpx, probably owing to a coupled substitution involving ^{IV}Al. Symbols are as in Fig. 10b. The error bars for D values are calculated using Monte Carlo simulation as described in the caption of Fig. 10.

The concentration of SiO_2 in the silicate liquid may also affect D_{Ti}, owing to its effect on the activity coefficient of TiO_2. As is well established from rutile-saturation experiments (Ryerson & Watson, 1987; Pertermann & Hirschmann, 2003*a*), silica enrichment raises $\gamma_{TiO_2}^{Ls}$. Thus, the low silica concentration in the carbonated silicate liquids from our experiments leads to a low $\gamma_{TiO_2}^{Ls}$, and consequently to small D_{Ti}^{cpx-Ls} and D_{Ti}^{gt-Ls}. The low silica contents of the silicate liquids are in turn attributable partly to the effects of CO_2 (e.g. Kushiro, 1975). Enrichments in FeO* in the silicate liquids may further diminish $\gamma_{TiO_2}^{Ls}$, D_{Ti}^{cpx-Ls}, and D_{Ti}^{gt-Ls} (Xirouchakis *et al.*, 2001).

The crystal chemistry of cpx also influences D_{Ti}^{cpx-Ls}. As shown in Fig. 11, observed variations of D_{Ti}^{cpx-Ls} correlate with cpx Al_2O_3 content. This is probably due to coupled substitutions of Al_2O_3 and TiO_2 in cpx, presumably involving tetrahedral aluminium ($Ti^{4+} + 2Al^{3+} = Mg^{2+} + 2Si^{4+}$; e.g. Sepp & Kunzmann, 2001). Thus, the relatively low Al_2O_3 (low ^{IV}Al) in cpx from our experiments contributes to low values of D_{Ti}^{cpx-Ls}. However, we note that our observation of low D_{Ti}^{cpx-Ls} is favored at high pressures, as at lower pressures high ^{IV}Al promotes high Ti content in cpx and consequently higher values of D_{Ti}^{cpx-Ls} (e.g. Villiger *et al.*, 2004).

In summary, silicate partial melts of SLEC1 carbonated eclogite are highly enriched in TiO_2 owing to a combination of factors that reduce D_{Ti}^{cpx-Ls} and D_{Ti}^{gt-Ls}. These include low activity coefficients of TiO_2 in the silicate liquids, as a result of low SiO_2 and high FeO* and high TiO_2, and relatively low Al_2O_3 in pyroxene. These factors may well be realized in other carbonated partial melts of mafic lithologies, and therefore high-TiO_2 liquids may be produced over a wider range of pressures and bulk compositions than explored in this study.

Silica-undersaturated melt from carbonated eclogite vs alkalic OIBs

In Fig. 12, the major element characteristics of silicate melts generated from SLEC1 are compared with those of alkalic OIB and with melilitites from oceanic and continental localities. The SiO_2 contents of the partial melts are lower than most alkalic OIB and similar to or lower than those of natural melilitites and nephelinites. The partial melts also share other key compositional features with highly undersaturated lavas, including high FeO* and TiO_2, and low Al_2O_3. On its first appearance (ilmenite saturated), silicate melt is extremely rich in TiO_2 and FeO* and very low in Al_2O_3 compared with even the most extreme lava compositions. However, after ilmenite is exhausted, TiO_2 and FeO* contents of silicate partial melts decrease and Al_2O_3 and CaO contents increase rapidly with temperature from ~1300 to 1400 °C. Thus, at high melt fractions the partial melts closely match those of ocean island olivine melilitite with respect to all the major element oxides. They also have notable similarities to some of the less extreme (non-melilititic) alkalic lavas, including enrichments in FeO*, TiO_2, CaO and CaO/Al_2O_3, although the latter generally have higher SiO_2. The CaO contents of silicate partial melt from SLEC1 at moderate to high extent of melting (F >20 wt %) are high enough to match those of OIBs with HIMU signatures and of some melilitites. The similarity between the compositions of moderate- to high-degree melts of SLEC1 and some melilititic lavas invites the hypothesis that some of these lavas originate as partial melts of carbonated eclogite.

If some highly alkalic lavas originate from partial melting of SLEC1, the partial melts must be sufficiently primitive to be parental to the lavas. The moderate- to high-degree partial melts of SLEC1 have fairly high MgO contents (10–14 wt %) that are comparable with those of many primitive melilitites and other alkalic OIB. However, the natural lava compositions extend to even higher MgO concentrations (Fig. 12). If some of these highly magnesian lavas represent liquids, then they are unlikely to originate purely from partial melting of carbonated eclogite. However, the most MgO-rich alkali OIB and melilitites probably are affected by crystal accumulation, and so the MgO contents of their parental liquids are not well constrained.

Even if the partial melts of SLEC1 are plausible parental liquids for some melilitites, they clearly are too extreme in their composition to be the parents to most alkalic OIB. An alternative scenario is that partial melts of carbonated eclogite could be contributing

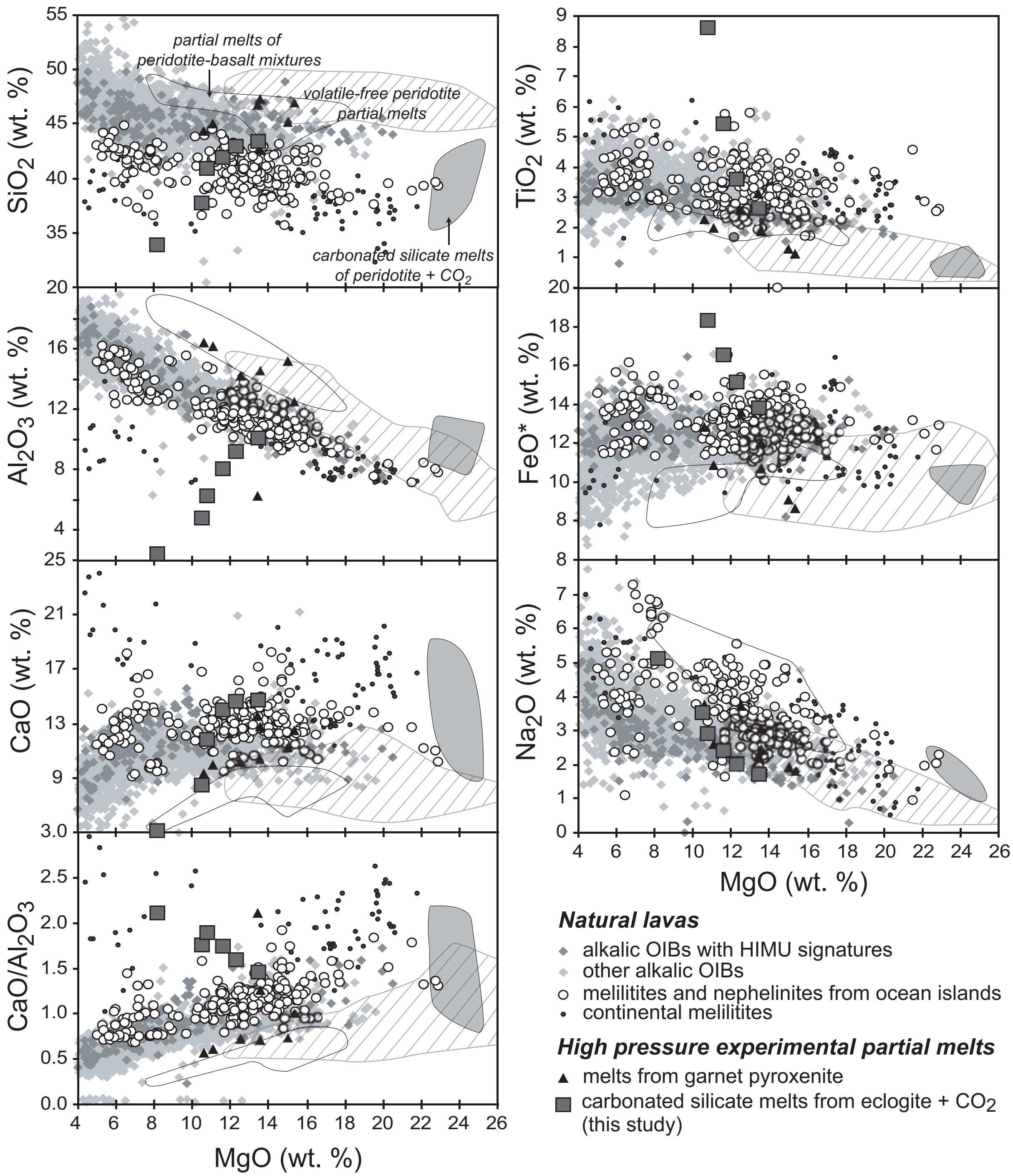

Fig. 12. Compositions of silicate-rich partial melts from SLEC1 (dark grey squares) compared with melilititic and nephelinitic lavas from ocean islands, melilititic lavas from continents, and other alkalic OIBs. High-pressure experimental partial melts from other mantle lithologies are also included. Data sources for natural lavas and experimental partial melts are as in Fig. 1.

components, rather than the primary source, of alkalic and highly alkalic OIB. Because the SLEC1 partial melts are rich in TiO_2 and FeO* and poor in Al_2O_3, mixtures between them and partial melts of peridotite $\pm$ CO_2 may produce liquids that match the compositions of many of the lavas.

A third scenario is that silicate partial melts of carbonated eclogite could metasomatize the surrounding mantle, yielding a fertile carbonated peridotite. Partial melts of such metasomatized carbonated peridotite may produce partial melts that more nearly match the compositional characteristics of natural alkalic lavas. In particular, such a process may yield lavas enriched in FeO* and TiO_2. It is less clear if such melts would be suitably poor in Al_2O_3 and enriched in CaO. Also, this scenario does not explain why inverse experiments failed to identify multiple saturation of primitive melilitites with natural garnet peridotite residua (Brey & Green, 1977; Brey, 1978; Brey & Ryabchikov, 1994).

Dynamics of melting of a heterogeneous carbonated mantle

The preceding discussion shows that silicate partial melts of carbonated eclogite such as SLEC1 have a number of compositional characteristics similar to alkalic and highly alkalic OIB. Furthermore, some of the compositional features of these partial melts, such as high TiO_2 and FeO* and low Al_2O_3, may potentially account for features of alkalic and highly alkalic OIB that are not easily explained by existing partial melting experiments on peridotite $\pm$ CO_2. If carbonated eclogites are present deep within the source of oceanic islands, they may be plausible sources of OIB or contribute to the sources of some OIB. However, evaluation of the potential of such melts to contribute to OIB petrogenesis also requires consideration of how such partial melts may form beneath oceanic islands under realistic geodynamic conditions.

A critical consideration is the conditions under which melting of carbonated eclogite may produce silicate melts. Our experiments demonstrate that such partial melts can be generated by batch melting of carbonated silica-deficient eclogite similar to SLEC1 at 3 GPa, corresponding to a depth of ~100 km, and between 1300 and 1400 °C. Although such conditions may be realized along geotherms that may occur in weak plumes or along the periphery of more vigorous plumes, it is less clear whether significant carbonate may remain in contact with eclogite at such depths. Along such a geotherm, carbonatitic liquids should be generated along the solidus of carbonated eclogite at much greater depths (Dasgupta *et al.*, 2004). Because such melts are likely to be highly mobile (Hunter & McKenzie, 1989; Minarik & Watson, 1995; Hammouda & Laporte, 2000), they might migrate out of their source eclogite bodies and into the surrounding peridotite; however, this depends partly on the relative rates of melting and compaction, which in turn depends on the size of the eclogite domain (Kogiso *et al.*, 2004*b*). If the carbonatite melt is expelled from the eclogite, its residue would probably not be a source for carbonated silicate partial melts. On the other hand, metasomatism of surrounding peridotite by carbonate melts from carbonated eclogite may create enriched sources capable of producing liquids similar to alkalic OIB. Also, if carbonatite melts escape eclogite sources at great depth, they may come into contact with devolatilized eclogite bodies at shallower depths, thereby leading to carbonated silicate melting of eclogite.

To understand the range of possible interactions between melts from different sources in a heterogeneous carbonated mantle, it is useful to consider the relative positions of solidi for likely lithologies. As illustrated in Fig. 13, the deepest melting should occur in bodies of carbonated eclogite, if they are present (Dasgupta *et al.*, 2004). Carbonatite melts expelled from carbonated eclogites may be implanted into surrounding carbonated peridotite. With further upwelling, the solidus of natural carbonated peridotite (Falloon & Green, 1989) is crossed, liberating carbonatite melts. These melts could originate either from the peridotite that has been metasomatized by melts of carbonated eclogite or from carbon that is endogenous in the peridotite. These carbonatite melts may then migrate upwards, percolating through both peridotite and any eclogite bodies they may encounter. A key consideration is that the carbonated silicate melts from our experiments are stable at lower temperatures than carbonated silicate melts in equilibrium with peridotite residue (Hirose, 1997). Thus, carbonatite melt, originating from carbonated eclogite or carbonated peridotite at depth, may percolate freely through peridotite, but there is a depth interval over which such melts will incite carbonated silicate melting when they encounter pyroxenite or eclogite bodies. Assuming that the onset of carbonated silicate melt stability in eclogite and peridotite follows temperature–pressure slopes similar to those of their respective volatile-free solidi (Hirschmann, 2000; Kogiso *et al.*, 2003), the carbonate-present silicate melting curve for eclogite intersects the oceanic geotherm between 4 and 5 GPa or a depth of 130–165 km, significantly shallower than the onset of stability of carbonatite in equilibrium with natural peridotite (i.e. Wallace & Green, 1988; Falloon & Green, 1989; Sweeney, 1994; Dasgupta *et al.*, 2005*b*), but deeper than the level at which such melts would induce silicate melting in peridotite. Thus, carbonated silicate melting of eclogite bodies may not be implausible, even though carbonatite melting may expel carbonate from eclogite at much greater depths.

Carbonated silicate melting of eclogite bodies would probably initiate at depths where carbonated silicate melts are not stable in peridotite. Such melts may migrate into surrounding peridotite, depending on the rates of melting and melt migration (Kogiso *et al.*, 2004*b*). If such melts migrate from the eclogite sources, they will solidify in the surrounding peridotite, producing a metasomatized peridotite that would begin to melt at yet shallower depths.

The scenarios described above suggest that the overall behaviour of a heterogeneous carbonated mantle

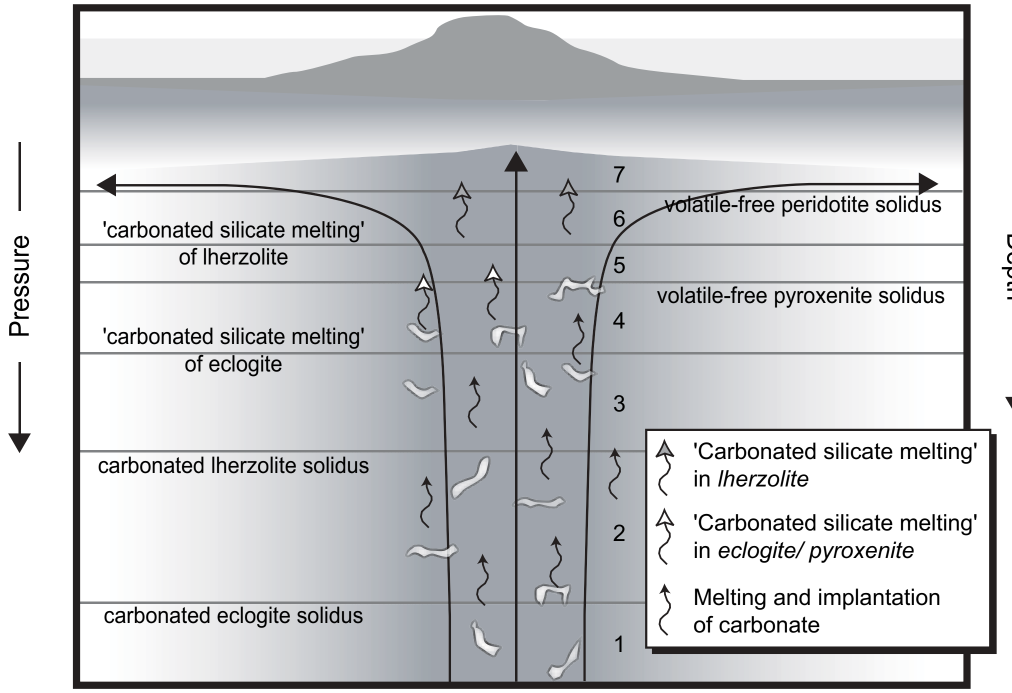

Fig. 13. Melting and metasomatism in upwelling carbonated oceanic mantle. At great depth (zone 1), CO_2 may be stored in peridotite and in eclogite or pyroxenite bodies (in white), if the latter are present. Above the solidus of carbonated eclogite (zone 2), highly mobile carbonatite melts generated from eclogite are likely to migrate into surrounding peridotite, where they will solidify as metasomatic carbonate. Thus, in zone 2, regions of peridotite may be carbonated, either owing to a pre-existing carbonaceous component present at depth or owing to recent metasomatism from proximal eclogite bodies. Once the carbonated peridotite solidus is crossed (zone 3), carbonatite melts may migrate freely through peridotite (and eclogite). In zone 4, migrating carbonatite liquids that intersect eclogite bodies will react to form carbonated silicate melts. If such melts migrate into the surrounding peridotite, they will solidify, forming metasomatized peridotite enriched in FeO, TiO_2 (+ incompatible trace elements). Carbonated silicate melting can commence in peridotite in zone 6. In the absence of CO_2, partial melting of eclogite or pyroxenite and peridotite will commence in zones 5 and 7, respectively. Delivery to the lithosphere of carbonatite liquids requires limited reaction with eclogite in zone 4 and above and with peridotite in zone 6 and above. Delivery to the lithosphere of carbonated silicate melts from eclogite requires limited reaction with peridotite in zones 4 and above. The positions of solidi in this diagram are schematic; however, their relative placements are constrained by the following studies: volatile-free peridotite: Hirschmann (2000); volatile-free pyroxenite: Yasuda *et al.* (1994), Pertermann & Hirschmann (2003*b*); carbonated lherzolite: Falloon & Green (1989); carbonated eclogite: Dasgupta *et al.* (2004). Carbonated silicate melting of eclogite is from the present study and carbonated silicate melting of lherzolite is from Hirose (1997). In general, the location of each of these solidi varies with bulk-rock composition (Hirschmann, 2000; Kogiso *et al.*, 2004*a*; Dasgupta *et al.*, 2005*a*); thus, we expect the real solidus boundaries to vary locally.

involves repeated melting of heterogeneities, metasomatism of surrounding, more refractory peridotite, followed by partial melting of the metasomatized region. Because of the very different solidi for production of carbonatite melts and of carbonated silicate melts, some regions of the mantle may experience multiple stages of melting, metasomatism, and remelting. The effect on highly incompatible trace elements may be large, resulting in strong enrichments. These scenarios deserve further investigation.

ACKNOWLEDGEMENTS

R.D. acknowledges support from V. R. Murthy & J. Noruk fellowship and a Doctoral Dissertation fellowship of the University of Minnesota during course of this study. We thank Rachel Dwarzski and Dave Draper for permission to cite their unpublished data, and Cyril Aubaud and Fred Frey for valuable discussions. Bob Luth, Peter Ulmer, and an anonymous reviewer are gratefully acknowledged for their constructive and thorough reviews. This work is supported by National Science Foundation grant EAR-0310142 to M.M.H. Kate Stalker's summer internship at Minnesota was funded through the University of Minnesota, Department of Geology & Geophysics, REU site, National Science Foundation grant EAR-0243526.

REFERENCES

Allègre, C. J., Pineau, F., Bernat, M. & Javoy, M. (1971). Evidence for the occurrence of carbonatites on the Cape Verde and Canary islands. *Nature* **233**, 103–104.

Alt, J. C. & Teagle, D. A. H. (1999). The uptake of carbon during alteration of ocean crust. *Geochimica et Cosmochimica Acta* **63**, 1527–1535.

Baker, M. B. & Wyllie, P. J. (1990). Liquid immiscibility in a nephelinite–carbonate system at 25 kbar and implications for carbonatite origin. *Nature* **346**, 168–170.

Blank, J. G. & Brooker, R. A. (1994). Experimental studies of carbon dioxide in silicate melts: solubility, speciation, and stable carbon isotope behavior. In: Caroll, M. R. & Holloway, J. R. (eds) *Volatiles in Magmas*. Washington, DC: Mineralogical Society of America, pp. 157–186.

Brey, G. (1978). Origin of olivine melilitites—chemical and experimental constraints. *Journal of Volcanology and Geothermal Research* **3**, 61–88.

Brey, G. & Green, D. H. (1975). The role of CO_2 in the genesis of olivine melilitite. *Contributions to Mineralogy and Petrology* **49**, 93–103.

Brey, G. P. & Green, D. H. (1976). Solubility of CO_2 in olivine melilitite at high pressures and role of CO_2 in Earth's upper mantle. *Contributions to Mineralogy and Petrology* **55**, 217–230.

Brey, G. & Green, D. H. (1977). Systematic study of liquidus phase relations in olivine melilitite + H_2O + CO_2 at high pressures and petrogenesis of an olivine melilitite magma. *Contributions to Mineralogy and Petrology* **61**, 141–162.

Brey, G. P. & Ryabchikov, I. D. (1994). Carbon dioxide in strongly silica undersaturated melts and origin of kimberlite magmas. *Neues Jahrbuch für Mineralogie, Monatshefte* **10**, 449–463.

Brooker, R. A. (1998). The effect of CO_2 saturation on immiscibility between silicate and carbonate liquids: an experimental study. *Journal of Petrology* **39**, 1905–1915.

Brooker, R. A., Kohn, S. C., Holloway, J. R., McMillan, P. F. & Carroll, M. R. (1999). Solubility, speciation and dissolution mechanisms for CO_2 in melts on the $NaAlO_2-SiO_2$ join. *Geochimica et Cosmochimica Acta* **63**, 3549–3565.

Brooker, R. A., Kohn, S. C., Holloway, J. R. & McMillan, P. F. (2001). Structural controls on the solubility of CO_2 in silicate melts Part I: bulk solubility data. *Chemical Geology* **174**, 225–239.

Caroff, M., Maury, R. C., Guille, G. & Cotten, J. (1997). Partial melting below Tubuai (Austral Islands, French Polynesia). *Contributions to Mineralogy and Petrology* **127**, 369–382.

Clague, D. A. & Frey, F. A. (1982). Petrology and trace element geochemistry of the Honolulu volcanics, Oahu: implications for the oceanic mantle below Hawaii. *Journal of Petrology* **23**, 447–504.

Clague, D. A. & Dalrymple, G. B. (1988). Age and petrology of alkalic postshield and rejuvenated-stage lava from Kauai, Hawaii. *Contributions to Mineralogy and Petrology* **99**, 202–218.

Coltorti, M., Bonadiman, C., Hinton, R. W., Siena, F. & Upton, B. G. J. (1999). Carbonatitic metasomatism of the oceanic upper mantle: evidence from clinopyroxenes and glasses in ultramafic xenoliths of Grande Comore, Indian Ocean. *Journal of Petrology* **40**, 133–165.

Dalton, J. A. & Presnall, D. C. (1998). The continuum of primary carbonatitic–kimberlitic melt compositions in equilibrium with lherzolite: data from the system $CaO-MgO-Al_2O_3-SiO_2-CO_2$ at 6 GPa. *Journal of Petrology* **39**, 1953–1964.

Dasgupta, R., Hirschmann, M. M. & Withers, A. C. (2004). Deep global cycling of carbon constrained by the solidus of anhydrous, carbonated eclogite under upper mantle conditions. *Earth and Planetary Science Letters* **227**, 73–85.

Dasgupta, R., Hirschmann, M. M. & Dellas, N. (2005*a*). The effect of bulk composition on the solidus of carbonated eclogite from partial melting experiments at 3 GPa. *Contributions to Mineralogy and Petrology* **149**, 288–305.

Dasgupta, R., Hirschmann, M. M. & Withers, A. C. (2005*b*). Near-solidus melt compositions from natural carbonated lherzolite. *Geochimica et Cosmochimica Acta* 69(**10S**), A101.

Dawson, J. B., Smith, J. V. & Jones, A. P. (1985). A comparative study of bulk rock and mineral chemistry of olivine melilitites and associated rocks from East and South Africa. *Neues Jahrbuch für Mineralogie, Abhandlungen* **152**, 143–175.

Demény, A., Vennemann, T. W., Hegner, E., Ahijado, A., Casillas, R., Nagy, G., Homonnay, Z., Gutierrez, M. & Szabó, C. (2004). H, O, Sr, Nd, and Pb isotopic evidence for recycled oceanic crust in the Transitional Volcanic Group of Fuerteventura, Canary Islands, Spain. *Chemical Geology* **205**, 37–54.

Dickinson, J. E. & Hess, P. C. (1985). Rutile solubility and titanium coordination in silicate melts. *Geochimica et Cosmochimica Acta* **49**, 2289–2296.

Dixon, J. E. (1997). Degassing of alkalic basalts. *American Mineralogist* **82**, 368–378.

Dixon, J. E., Clague, D. A., Wallace, P. & Poreda, R. (1997). Volatiles in alkalic basalts from the North Arch volcanic field, Hawaii: extensive degassing of deep submarine-erupted alkalic series lavas. *Journal of Petrology* **38**, 911–939.

Doucelance, R., Escrig, S., Moreira, M., Gariepy, C. & Kurz, M. D. (2003). Pb−Sr−He isotope and trace element geochemistry of the Cape Verde Archipelago. *Geochimica et Cosmochimica Acta* **67**, 3717–3733.

Dupuy, C., Barsczus, H. G., Liotard, J. M. & Dostal, J. (1988). Trace element evidence for the origin of ocean island basalts: an example from the Austral Islands (French Polynesia). *Contributions to Mineralogy and Petrology* **98**, 293–302.

Dupuy, C., Barsczus, H. G., Dostal, J., Vidal, P. & Liotard, J.-M. (1989). Subducted and recycled lithosphere as the mantle source of ocean island basalts from southern Polynesia, central Pacific. *Chemical Geology* **77**, 1–18.

Dwarzski, R. E. & Draper, D. S. (2004). Effect of titanium on REE and HFSE partitioning between garnet and melt. *EOS Trans. Fall Meeting Suppl.* **85**(47), F1887.

Eggler, D. H. (1978). The effect of CO_2 upon partial melting of peridotite in the system $Na_2O-CaO-Al_2O_3-MgO-SiO_2-CO_2$ to 35 kb, with an analysis of melting in a peridotite–H_2O-CO_2 system. *American Journal of Science* **278**, 305–343.

Eggler, D. H. & Mysen, B. O. (1976). The role of CO_2 in the genesis of olivine melilitite: discussion. *Contributions to Mineralogy and Petrology* **55**, 231–236.

Ellis, D. J. & Green, D. H. (1979). An experimental study of the effect of Ca upon garnet–clinopyroxene Fe–Mg exchange equilibria. *Contributions to Mineralogy and Petrology* **71**, 13–22.

Falloon, T. J. & Green, D. H. (1989). The solidus of carbonated, fertile peridotite. *Earth and Planetary Science Letters* **94**, 364–370.

Frey, F. A., Green, D. H. & Roy, S. D. (1978). Integrated models of basalt petrogenesis: a study of quartz tholeiites to olivine melilitities from south eastern Australia utilizing geochemical and experimental petrological data. *Journal of Petrology* **19**, 463–513.

Green, D. H. & Falloon, T. J. (1998). Pyrolite: a Ringwood concept and its current expression. In: Jackson, I. (ed.) *The Earth's Mantle: Composition, Structure, and Evolution*. Cambridge: Cambridge University Press, pp. 311–378.

Gudfinnsson, G. H. & Presnall, D. C. (2005). Continuous gradations among primary carbonatitic, kimberlitic, melilititic, basaltic, picritic, and komatiitic melts in equilibrium with garnet lherzolite at 3–8 GPa. *Journal of Petrology* **46**, 1645–1659.

Hammouda, T. (2003). High-pressure melting of carbonated eclogite and experimental constraints on carbon recycling and storage in the mantle. *Earth and Planetary Science Letters* **214**, 357–368.

Hammouda, T. & Laporte, D. (2000). Ultrafast mantle impregnation by carbonatite melts. *Geology* **28**, 283–285.

Hauri, E. H., Shimizu, N., Dieu, J. J. & Hart, S. R. (1993). Evidence for hotspot-related carbonatite metasomatism in the oceanic upper mantle. *Nature* **365**, 221–227.

Hawkins, J. W., Jr & Natland, J. H. (1975). Nephelinites and basanites of the Samoan linear volcanic chain: their possible tectonic significance. *Earth and Planetary Science Letters* **24**, 427–439.

Hegner, E., Walter, H. J. & Satir, M. (1995). Pb–Sr–Nd isotopic compositions and trace element geochemistry of megacrysts and melilitites from the Tertiary Urach volcanic field: source composition of small volume melts under SW Germany. *Contributions to Mineralogy and Petrology* **122**, 322–335.

Hémond, C., Devey, C. W. & Chauvel, C. (1994). Source compositions and melting processes in the Society and Austral plumes (South Pacific Ocean): element and isotope (Sr, Nd, Pb, Th) geochemistry. *Chemical Geology* **115**, 7–45.

Herzberg, C. & O'Hara, M. J. (2002). Plume-associated ultramafic magmas of Phanerozoic age. *Journal of Petrology* **43**, 1857–1883.

Hirose, K. (1997). Partial melt compositions of carbonated peridotite at 3 GPa and role of CO_2 in alkali-basalt magma generation. *Geophysical Research Letters* **24**, 2837–2840.

Hirose, K. & Kushiro, I. (1993). Partial melting of dry peridotites at high pressures: determination of compositions of melts segregated from peridotite using aggregates of diamond. *Earth and Planetary Science Letters* **114**, 477–489.

Hirschmann, M. M. (2000). The mantle solidus: experimental constraints and the effect of peridotite composition. *Geochemistry, Geophysics, Geosystems* **1**, 2000GC000070.

Hirschmann, M. M., Kogiso, T., Baker, M. B. & Stolper, E. M. (2003). Alkalic magmas generated by partial melting of garnet pyroxenite. *Geology* **31**(6), 481–484.

Hoernle, K. & Schmincke, H.-U. (1993). The petrology of the tholeiites through melilite nephelinites on Gran Canaria, Canary Islands: crystal fractionation, accumulation, and depths of melting. *Journal of Petrology* **34**, 573–597.

Hoernle, K., Tilton, G. & Schmincke, H.-U. (1991). Sr–Nd–Pb isotopic evolution of Gran Canaria: evidence for shallow enriched mantle beneath the Canary Islands. *Earth and Planetary Science Letters* **106**, 44–63.

Hoernle, K., Tilton, G., Le Bas, M. J., Duggen, S. & Schönberg, D. G. (2002). Geochemistry of oceanic carbonatites compared with continental carbonatites: mantle recycling of oceanic crustal carbonate. *Contributions to Mineralogy and Petrology* **142**, 520–542.

Hunter, R. H. & McKenzie, D. (1989). The equilibrium geometry of carbonate melts in rocks of mantle composition. *Earth and Planetary Science Letters* **92**, 347–356.

Ivanikov, V. V., Rukhlov, A. S. & Bell, K. (1998). Magmatic evolution of the melilitite–carbonatite–nephelinite dyke series of the Tury peninsula (Kandalaksha Bay, White Sea, Russia). *Journal of Petrology* **39**, 2043–2059.

Janney, P. E., Le Roex, A. P., Carlson, R. W. & Viljoen, K. S. (2002). A chemical and multi-isotope study of the western Cape olivine melilititic province, South Africa: implications for the sources of kimberlites and the origin of the HIMU signature in Africa. *Journal of Petrology* **43**, 2339–2370.

Jørgensen, J. Ø. & Holm, P. M. (2002). Temporal variation and carbonatite contamination in primitive ocean island volcanics from São Vicente, Cape Verde Islands. *Chemical Geology* **192**, 249–267.

Keshav, S., Gudfinnsson, G. H., Sen, G. & Fei, Y. (2004). High-pressure melting experiments on garnet clinopyroxenite and the alkalic to tholeiitic transition in ocean island basalts. *Earth and Planetary Science Letters* **223**, 365–379.

Kjarsgaard, B. A. (1998). Phase relations of a carbonated high-CaO nephelinite at 0·2 and 0·5 GPa. *Journal of Petrology* **39**, 2061–2075.

Kjarsgaard, B. A., Hamilton, D. L. & Peterson, T. D. (1995). Peralkaline nephelinite/carbonatite liquid immiscibility: comparison of phase compositions in experiments and natural lavas from Oldoinyo Lengai. In: Bell, K. & Keller, J (eds) *Carbonatite Volcanism Oldoinyo Lengai and the Petrogenesis of Natrocarbonatite*. Berlin: Springer, pp. 163–190.

Kogarko, L. N., Kurat, G. & Ntaflos, T. (2001). Carbonate metasomatism of the oceanic mantle beneath Fernando de Noronha Island, Brazil. *Contributions to Mineralogy and Petrology* **140**, 577–587.

Kogiso, T., Tatsumi, Y., Shimoda, G. & Barsczus, G. (1997). High μ (HIMU) ocean island basalts in southern Polynesia: new evidence for whole mantle scale recycling of subducted oceanic crust. *Journal of Geophysical Research* **102**, 8085–8103.

Kogiso, T., Hirose, K. & Takahashi, E. (1998). Melting experiments on homogeneous mixtures of peridotite and basalt: application to the genesis of ocean island basalts. *Earth and Planetary Science Letters* **162**, 45–61.

Kogiso, T., Hirschmann, M. M. & Frost, D. J. (2003). High-pressure partial melting of garnet pyroxenite: possible mafic lithologies in the source of ocean island basalts. *Earth and Planetary Science Letters* **216**, 603–617.

Kogiso, T., Hirschmann, M. M. & Pertermann, M. (2004*a*). High-pressure partial melting of mafic lithologies in the mantle. *Journal of Petrology* **45**, 2407–2422.

Kogiso, T., Hirschmann, M. M. & Reiners, P. W. (2004*b*). Length scales of mantle heterogeneities and their relationship to ocean island basalt geochemistry. *Geochimica et Cosmochimica Acta* **68**, 345–360.

Krogh-Ravna, E. (2000). The garnet–clinopyroxene Fe^{2+}–Mg geothermometer: an updated calibration. *Journal of Metamorphic Geology* **18**, 211–219.

Kubicki, J. D. & Stolper, E. M. (1995). Structural roles of CO_2 and $[CO_3]^{2-}$ in fully polymerized sodium aluminosilicate melts and glasses. *Geochimica et Cosmochimica Acta* **59**, 683–698.

Kushiro I. (1975). On the nature of silicate melt and its significance in magma genesis: regularities in the shift of the liquidus boundaries involving olivine, pyroxene, and silica minerals. *American Journal of Science* **275**, 411–431.

Kushiro, I. (1996). Partial melting of a fertile mantle peridotite at high pressures: an experimental study using aggregates of diamond. In: Basu, A. & Hart, S. (eds) *Earth Processes: Reading the Isotopic Code*. Washington, DC: American Geophysical Union, pp. 109–122.

Le Bas, M. J. (1989). Nephelinitic and basanitic rocks. *Journal of Petrology* **30**, 1299–1312.

Lee, W.-J. & Wyllie, P. J. (1997). Liquid immiscibility between nephelinite and carbonatite from 1·0 to 2·5 GPa compared with mantle melt compositions. *Contributions to Mineralogy and Petrology* **127**, 1–16.

Longhi, J. (2002). Some phase equilibrium systematics of lherzolite melting: I. *Geochemistry, Geophysics, Geosystems* **3**, 2001GC000204.

Maaløe, S., James, D., Smedley, P., Petersen, S. & Garmann, L. B. (1992). The Kola volcanic suite of Kauai, Hawaii. *Journal of Petrology* **33**, 761–784.

Minarik, W. G. & Watson, E. B. (1995). Interconnectivity of carbonate melt at low melt fraction. *Earth and Planetary Science Letters* **133**, 423–437.

Moore, K. R. & Wood, B. J. (1998). The transition from carbonate to silicate melts in the $CaO-MgO-SiO_2-CO_2$ system. *Journal of Petrology* **39**, 1943–1951.

Nakamura, K. & Kato, Y. (2004). Carbonatization of oceanic crust by the seafloor hydrothermal activity and its significance as a CO_2 sink in the Early Archean. *Geochimica et Cosmochimica Acta* **68**, 4595–4618.

Neumann, E.-R., Wulff-Pedersen, E., Pearson, N. J. & Spencer, E. A. (2002). Mantle xenoliths from Tenerife (Canary Islands): evidence for reactions between mantle peridotites and silicic carbonatite melts inducing Ca metasomatism. *Journal of Petrology* **43**, 825–857.

Nielsen, T. F. D., Solovova, I. P. & Veksler, I. V. (1997). Parental melts of melilitolite and origin of alkaline carbonatite: evidence from crystallised melt inclusions, Gardiner complex. *Contributions to Mineralogy and Petrology* **126**, 331–344.

Nougier, J., Cantagrel, J. M. & Carche, J. P. (1986). The Comores archipelago in the Western Indian Ocean: volcanology, geochronology and geodynamic setting. *Journal of African Earth Science* **5**, 135–145.

O'Hara, M. J. (1968). The bearing of phase equilibria studies in synthetic and natural systems on the origin and evolution of basic and ultrabasic rocks. *Earth-Science Reviews* **4**, 69–133.

Oversby, V. M. (1971). Lead in oceanic islands: Faial, Azores and Trindade. *Earth and Planetary Science Letters* **11**, 401–406.

Palacz, Z. A. & Saunders, A. D. (1986). Coupled trace element and isotope enrichment in the Cook–Austral–Samoa islands, Southwest Pacific. *Earth and Planetary Science Letters* **79**, 270–280.

Pertermann, M. & Hirschmann, M. M. (2002). Trace-element partitioning between vacancy-rich eclogitic clinopyroxene and silicate melt. *American Mineralogist* **87**, 1365–1376.

Pertermann, M. & Hirschmann, M. M. (2003*a*). Anhydrous partial melting experiments on MORB-like eclogite: phase relations, phase compositions and mineral–melt partitioning of major elements at 2–3 GPa. *Journal of Petrology* **44**, 2173–2201.

Pertermann, M. & Hirschmann, M. M. (2003*b*). Partial melting experiments on a MORB-like pyroxenite between 2 and 3 GPa: constraints on the presence of pyroxenite in basalt source regions from solidus location and melting rate. *Journal of Geophysical Research* **108**(2125), doi:10.1.29/2000JB000118.

Pertermann, M., Hirschmann, M. M., Hametner, K., Günther, D. & Schmidt, M. (2004). Experimental determination of trace element partitioning between garnet and silica-rich liquid during anhydrous partial melting of MORB-like eclogite. *Geochemistry, Geophysics, Geosystems* **5**(Q05A01), doi:10.1029/2003GC000638.

Presnall, D. C., Gudfinnsson, G. H. & Walter, M. J. (2002). Generation of mid-ocean ridge basalts at pressures from 1 to 7 GPa. *Geochimica et Cosmochimica Acta* **66**, 2073–2090.

Ryerson, F. J. & Watson, E. B. (1987). Rutile saturation in magmas: implications for Ti–Nb–Ta depletion in island-arc basalts. *Earth and Planetary Science Letters* **86**, 225–239.

Saal, A. E., Hart, S. R., Shimizu, N., Hauri, E. H. & Layne, G. D. (1998). Pb isotopic variability in melt inclusions from oceanic island basalts, Polynesia. *Science* **282**, 1481–1484.

Schultz, F., Lehman, B. Tawackoli, S., Rossling, R. Belyatski, B. & Dulski, P. (2004). Carbonatite diversity in the Central Andes: the Ayopaya alkaline province, Bolivia. *Contributions to Mineralogy and Petrology* **148**, 391–408.

Sepp, B. & Kunzmann, T. (2001). The stability of clinopyroxene in the system $CaO-MgO-SiO_2-TiO_2$ (CMST). *American Mineralogist* **86**, 265–270.

Späth, A., Le Roex, A. P. L. & Duncan, R. A. (1996). The geochemistry of lavas from the Comores Archipelago, Western Indian Ocean: petrogenesis and mantle source region characteristics. *Journal of Petrology* **37**, 961–991.

Sweeney, R. J. (1994). Carbonatite melt compositions in the Earth's mantle. *Earth and Planetary Science Letters* **128**, 259–270.

Takahashi, E. (1986). Melting of a dry peridotite KLB-1 up to 14 GPa: implications on the origin of peridotitic upper mantle. *Journal of Geophysical Research* **91**, 9367–9382.

Takahashi, E. & Kushiro, I. (1983). Melting of a dry peridotite at high pressures and basalt magma genesis. *American Mineralogist* **68**, 859–879.

Thibault, Y. & Holloway, J. R. (1994). Solubility of CO_2 in a Ca-rich leucitite: effects of pressure, temperature, and oxygen fugacity. *Contributions to Mineralogy and Petrology* **116**, 216–224.

Van Orman, J. A. & Grove, T. L. (2000). Origin of lunar high-titanium ultramafic glasses: constraints from phase relations and dissolution kinetics of clinopyroxene–ilmenite cumulates. *Meteoritics and Planetary Sciences* **35**, 783–794.

Villiger, S., Ulmer, P., Müntener, O. & Thompson, A. B. (2004). The liquid line of descent of anhydrous, mantle-derived, tholeiitic liquids by fractional and equilibrium crystallization—an experimental study at 1·0 GPa. *Journal of Petrology* **45,** 2369–2388.

Wallace, M. E. & Green, D. H. (1988). An experimental determination of primary carbonatite magma composition. *Nature* **335**, 343–346.

Walter, M. J. (1998). Melting of garnet peridotite and the origin of komatiite and depleted lithosphere. *Journal of Petrology* **39**, 29–60.

Walter, M. J., Sisson, T. W. & Presnall, D. C. (1995). A mass proportion method for calculating melting reactions and application to melting of model upper mantle lherzolite. *Earth and Planetary Science Letters* **135**, 77–90.

Weaver, B. L. (1990). Geochemistry of highly-undersaturated ocean island basalt suites from South Atlantic Ocean: Fernando de Noronha and Trindade islands. *Contributions to Mineralogy and Petrology* **105**, 502–515.

Wilson, M., Rosenbaum, J. M. & Dunworth, E. A. (1995). Melilitites: partial melts of the thermal boundary layer? *Contributions to Mineralogy and Petrology* **119**, 181–196.

Workman, R. K., Hart, S. R., Jackson, M., Regelous, M., Farley, K. A., Blusztajn, J., Kurz, M. & Staudigel, H. (2004). Recycled metasomatized lithosphere as the origin of the Enriched Mantle II (EM2) end-member: evidence from the Samoan Volcanic Chain. *Geochemistry, Geophysics, Geosystems* **5**(Q04008), doi:10.1029/2003GC000623.

Xirouchakis, D., Hirschmann, M. M. & Simpson, J. A. (2001). The effect of titanium on the silica content and on mineral–liquid partitioning of mantle-equilibrated melts. *Geochimica et Cosmochimica Acta* **65**, 2201–2217.

Yasuda, A., Fujii, T. & Kurita, K. (1994). Melting phase relations of anhydrous mid-ocean ridge basalt from 3 to 20 GPa: implications for the behavior of subducted oceanic crust in the mantle. *Journal of Geophysical Research* **99**, 9401–9414.

Yaxley, G. M. & Brey, G. P. (2004). Phase relations of carbonate-bearing eclogite assemblages from 2·5 to 5·5 GPa: implications for petrogenesis of carbonatites. *Contributions to Mineralogy and Petrology* **146**, 606–619.

Yaxley, G. M. & Green, D. H. (1996). Experimental reconstruction of sodic dolomitic carbonatite melts from metasomatised lithosphere. *Contributions to Mineralogy and Petrology* **124**, 359–369.

Yaxley, G. M. & Green, D. H. (1998). Reactions between eclogite and peridotite: mantle refertilization by subduction of oceanic crust. *Schweizerische Mineralogische und Petrographische Mitteilungen* **78**, 243–255.